Accepted Manuscript

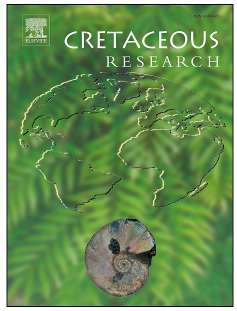

Change from rimmed to ramp platform forced by regional and global events in the Cretaceous of the Friuli-Adriatic Platform (Southern Alps, Italy)

Vincenzo Picotti, Miriam Cobianchi, Valeria Luciani, Franziska Blattmann, Tanja Schenker, Erica Mariani, Stefano M. Bernasconi, Helmut Weissert

PII: S0195-6671(19)30107-7

DOI: https://doi.org/10.1016/j.cretres.2019.07.007

Reference: YCRES 4177

To appear in: *Cretaceous Research*

Received Date: 13 March 2019

Revised Date: 10 June 2019

Accepted Date: 6 July 2019

Change from rimmed to ramp platform forced by regional and global events in the Cretaceous of the Friuli-Adriatic Platform (Southern Alps, Italy)

Vincenzo Picotti [a *], Miriam Cobianchi [b], Valeria Luciani [c], Franziska Blattmann [a,d] Tanja Schenker [a], Erica Mariani [b,e], Stefano M. Bernasconi [a], Helmut Weissert [a]

[a] Department of Earth Sciences, Geological Institute, ETH Zurich, Sonneggstrasse 5, 8092 Zürich, Switzerland

[b] Dipartimento di Scienze della Terra e dell’Ambiente, Università degli Studi di Pavia, via Ferrata 1, I-27100 Pavia, Italy

[c] Dipartimento di Fisica e Scienze della Terra, Università degli Studi di Ferrara, via Saragat 1, I-44121 Ferrara

[d] Faculty of Geosciences and Environment, Institute of Earth Surface Dynamics, Quartier UNIL, Bâtiment Géopolis, CH-1015 Lausanne.

[e] Camborne School of Mines, College of Engineering, Mathematics and Physical Sciences, University of Exeter, Penryn Campus, Treliever Road, Penryn, Cornwall TR10 9FE, United Kingdom

Abstract

Carbonate platforms are sedimentary archives recording the evolution of the global carbon cycle. Their stratigraphic architecture depends on the regional tectonics, controlling subsidence rates and geometries, as well as the paleoceanography and evolutionary trends, controlling the different organisms thriving at their margins, such as frame-building corals or mound-building microbes. We present an integrated bio- and chemostratigraphic study of the Aptian to Santonian interval of a base-of-slope section located in the Southern Alps of northeastern Italy that we correlate with the classic section representing the Friuli-Adriatic Carbonate Platform, one of the largest isolated platforms of the low latitude Tethys. We show the effects of the end of the passive-margin stage and the interaction between foreland flexuring due to the growing Alps, to which the study area represented the retroforeland, and the approaching prowedge of the Dinarides. The Friuli-Adriatic platform margin shows an abrupt change from reef rimmed to ramp, where abundant microbial mounds provided the habitat for the rudists to thrive. This change occurred around the late Albian and likely correlates with the Oceanic Anoxic Event (OAE) 1d. The previous OAE’s did not change the structure of this platform, whose margins were mostly rigid and colonized by corals and calcareous sponges. Late Albian was a time of important changes in paleoceanography in Tethys

and North Atlantic Oceans. We propose that the paleooceanographic changes related to the OAE-1d had more profound impacts on the Friuli-Adriatic Platform than the previous Cretaceous OAE's since they co-occurred with the tectonic transition from passive margin to foreland ramp. The increased subsidence rates, in conjuction with the important late Albian paleoceanographic changes, created favourable conditions for a dramatic change in the platform margin physiography and ecology.

Highlights

- Correlation of a carbonate platform with its base-of-slope by integrating nanno and foraminifera bio- and chemostratigraphy.
- At the late Albian, the slope changed from sediment-starved to gravity flows supplied; the platform margin changed from rimmed to ramp.
- Corals and calcareous sponges were replaced by rudists and microbes forming large mounds.
- Alpine/Dinaric foreland tectonics and the environmental stress related to the OAE1d controlled this abrupt change.

Keywords
Cretaceous Oceanic Anoxic Events; calcareous nannofossils; foraminifera; stable Carbon isotopes; platform margin; alpine/dinaric foreland basin.

*Corresponding author vincenzo.picotti@erdw.ethz.ch

1. Introduction

The response of the carbonate platforms to the mid-Cretaceous Oceanic Anoxic Events (OAEs, e.g. Schlanger and Jenkyns 1976) was not univocal, and varied depending on their paleoceanographic and tectonic setting. The most common responses include platform drowning, more or less partially, or simply carbonate factory shift from Photozoan to Heterozoan (e.g. Schlager, 2003; Mutti and Hallock, 2003). These important changes in the structure and architecture of carbonate platforms are considered as a consequence of the strong oceanographic perturbations associated to OAEs, including ocean temperature and acidity and nutrient input (e.g. Jenkyns, 1991; Phelps et al., 2015). The Tethyan isolated platforms were less sensitive than rimmed platforms to the hyperthermal conditions and associated perturbations (e.g. Weissert et al., 1998; Amodio and Weissert, 2017). Some authors proposed a "kettle effect" on shallow water banks (e.g. Skelton and Gili, 2012), when ocean acidification trends were compensated by thermal CO_2 expulsion from the extremely warm surface waters.

For this study, we selected the Tethyan Cretaceous Friuli-Adriatic Carbonate Platform margin (northwestern Italy) for an investigation of relationships between platform growth, tectonics and global climate. The Friuli-Adriatic Carbonate Platform (Fig. 1) is of particular interest as it represents the northwest edge of one of the largest Cretaceous Tethyan platforms, the Adriatic Carbonate Platform (AdCP - Vlahović et al., 2005). Its northwest margins and slope are well exposed in the Southern Alps of Italy (Picotti and Cobianchi, 2017) and its northeast margin in central Croatia (e.g. Pamić et al., 1998). On the contrary, the southeastern edge of the platform is recorded in the subsurface Adriatic area (e.g. Masetti et al., 2012). The time interval selected is of particular interest as the Cretaceous is known as being marked by significant changes in the global carbon cycle and related paleoceanographic events testified by widespread deposition of organic-rich shales that are the sedimentary expression of OAEs (Schlanger and Jenkyns, 1976). The OAEs, according to available data (e.g. Bralower et al., 1995; Larson and Erba, 1999; Weissert and Erba, 2004; Föllmi et al., 2006; Föllmi 2012; Jenkyns et al., 2017; Jenkyns, 2018), were largely triggered by massive pulses of submarine mafic volcanism accompanying the emplacement of Large Igneous Provinces (LIPs), especially intense for the Aptian OAE1a (Selli event) and the latest Cenomanian OAE2 (Bonarelli event) (e.g. Kidder and Worsley, 2010). Volcanic activity turned the climate into a hothouse mode (sensu Kidder and Worsley, 2010), accelerating continental weathering and increasing nutrient transfer from continents to oceans resulting in higher marine fertility (Weissert, 1989).

During the Cretaceous, growth and demise of carbonate platforms have been indeed related to carbon cycle pertubations as documented by bulk carbonate carbon isotope record ($\delta^{13}C$) (e.g. Föllmi et al., 2006; Jenkyns, 2010). Specifically, dramatic plaform demise and drowning events have been assigned to episodes of rapid increase of atmospheric CO_2, leading to ocean acidification that critically decreased saturation of calcium carbonate, which is essential for construction of marine organism shells, and enhanced nutrient input (e.g., Weissert et al., 1998; Wisler et al., 2003; Erba, 2004; Skelton and Gili, 2012: Honisch et al., 2012; Millán et al., 2014; Phelps et al., 2015). The LIPs emplacement, degassing large amounts of CO_2, inducing sea-level rise and accelerated continental runoff, are largely invoked as causing these carbonate platform growth crises (e.g. Wissler et al., 2003; Weissert and Erba, 2004; Jenkyns et al., 2017).

Our goal thereby is to describe the Cretaceous facies evolution of the Friuli-Adriatic platform and slope to unravel the possible impacts of the OAEs on its evolution. Papers dealing with the Cretaceous evolution of the Friuli Platform margin and adjacent Belluno Basin (Fig. 1) are relatively scarce and difficult to find (Ferasin, 1958; Ghetti, 1987; Schindler and Conrad, 1994; Woodfine, 2002).

Specifically, we examine the relationships between the evolution of the platform margin and the carbon cycle perturbations, as expressed by bulk sediment $\delta^{13}C$ record. Available Cretaceous marine $\delta^{13}C$ curves (e.g., Scholle and Arthur, 1980; Schlanger et al., 1987; Menegatti et al., 1998; Weissert et al., 1998; Stoll and Schrag, 2000; Luciani et al., 2004; Jarvis et al., 2006; Voigt et al., 2010; Millàn et al., 2009 and 2014; Coccioni and Premoli Silva, 2015; Thibault et al., 2016) show consistent trends among several provinces and provide sound basis for global correlation. Several positive and negative $\delta^{13}C$ shifts have been labelled (e.g., Jarvis et al., 2006) and linked to sea level changes and OAEs perturbations. A further aim is the definition of the main tectonic processes controlling the geometry and subsidence pattern of the platform, indeed considered as a good tracer of long-term tectonic regimes.

To attain our goals, we correlate the Val Cellina section (hereafter CE), a well-known platform succession (Cuvillier et al., 1968; Woodfine, 2002), with the base-of-slope Casso section (hereafter CS). The CE section has a solid biostratigraphic frame based on calcareous algae and benthic foraminifera (Bruni in Woodfine, 2002). In the following paragraphs, we present a new integrated stratigrahy of the CS section, previously described by Gnaccolini (1968) and Costacurta et al. (1979). We combine calcareous nannofossil, planktic and benthic foraminifera stratigraphy with bulk carbon and oxygen stable isotope stratigraphy. At the base of slope, resedimented periplatform deposits repeatedly interrupted the pelagic sedimentation. Pelagic sediments provide biostratigraphic information for dating resedimented deposits thus enabling the chronologically constrain of the platform events.

In detail, we focus on: 1 – an integrated bio- and chemostratigraphy at the base-of-slope of the Friuli- AdCP, to provide a frame of correlation with the platform and to highlight the Aptian, Albian and Cenomanian – Turonian Oceanic Anoxic Events, in absence of black shales preservation in the CS section; 2 – the tectonic evolution of the platform margin, including variations in the subsidence rates and the transition from passive margin to foreland ramp, and their consequences for the geometry of platform margin; 3 – the changes of the carbonate factory across the mid-Cretaceous and their relationships with the OAEs.

We demonstrate that the Friuli-Adriatic platform margin has been influenced by the transition from passive margin to foreland ramp (e.g. Pomar, 2001), due to the encroaching Alps and Dinarides. On the other hand, these tectonic changes have been enhanced by the abrupt variations of biota in the carbonate platform, forced by global paleoceanographic changes related to the OAEs.

2. Geological setting

The Friuli Platform (Fig. 1), westernmost promontory of the AdCP, bordered by the Belluno and Tolmin-Slovenian Basins, is a persistent shallow-water domain that developed at the proximal passive margin of the Adria microplate since the Late Triassic (e.g. Bernoulli and Jenkyns, 1974; Vlahović et al., 2005, Picotti and Cobianchi, 2017).

The western margin of the Adria microplate was rifting off Eurasia during the breakup of Pangea, eventually leading to the spreading of the Piedmont-Ligurian Ocean in the Middle Jurassic (Bertotti et al., 1993). The eastern margin of Adria, located several hundreds of km from the AdCP, was subducting since the Early Jurassic under Eurasia (e.g. Picotti and Cobianchi, 2017). This subduction of Adriatic lithosphere progressively created the Dinaric-Hellenic belt that encroached the AdCP in the Late Cretaceous to Paleogene (e.g. Auboin, 1970, Pamić et al., 1998). The Friuli-Adriatic Platform was involved first in the Dinaric fold and thrust belt, with flexuring, flysch deposition and thrusting toward the southwest (Cretaceous to Paleogene, e.g. Otoničar, 2007), and subsequently (Neogene) into the Alpine belt, with southeastward directed shortening (e.g. Mellere et al., 2000). The Friuli - Adriatic Platform during its passive margin stage in the Late Jurassic and Early Cretaceous underwent a homogenous subsidence that created an overall continuous succession all over its paleogeographic boundaries visible in Fig. 1. From the end Albian to Cenomanian, associated to the passive margin to foreland transition, the subsidence in the southern and western sector of the Friuli - Adriatic Platform abruptly stopped, as it is demonstrated by the persistent post Albian gap in the subsurface (wells Nervesa, Cesarolo) and outcrops in western Istria (Otoničar, 2007; Brčić et al., 2017), whereas other wells to the north and east show a more continuous Upper Cretaceous succession (Cargnacco and Grado, see ViDEPI and Cimolino et al., 2010). Underlying a prominent unconformity, covered by upper Oligocene to Lower Miocene glauconitic carbonates (Cavanella Group of the subsurface, e.g. Cimolino et al., 2010), the well Nervesa 001 at 2437 m from the rotary show late Albian ages with the occurrence of *Cuneolina pavonia parva* (ViDEPI). At Cesarolo 001, the same unconformity occurs at 727 m from the rotary, and the late Albian (early Cenomanian?) carbonates at the top still belong to the *Cuneolina pavonia parva* biozone (ViDEPI). The well Cargnacco 001 shows a more continuous Upper Cretaceous interval overlying the Albian carbonates, from 1570 to 1030 referred to the rotary. The shallow water carbonates continued in the Paleocene and Early Eocene, until they got covered by the terrigenous Flysch. At Grado, Cimolino et al. (2010) document a situation similar to Cargnacco 001, with Upper Cretaceous rudist carbonates followed by Paleocene to Eocene shallow water carbonates at 1015 to 622 m from rotary. Therefore, based on these subsurface data and the outcrops in Istria, it is possible to tentatively dash a boundary in the Friuli - Adriatic Platform, named post-Albian coastal onlap in Fig. 1, between the area with continuous upper Cretaceous and even Paleocene shallow-water sedimentation, and an area south and west of it, where the sedimentation stopped at the end of the Albian.

The studied sections Casso and Cellina (Fig. 1) are separated by thrusts and folds, whose minimum shortening was considered when providing the paleogeographic reconstructions in the next chapters, following available maps and sections (e.g. Riva et al., 1990).

The stratigraphy and sedimentology of the study area was investigated in the past, allowing the defininition of some relevant points for the architecture of the margin. Ferasin (1958) first described the main facies of platform, slope and basin, and proposed a simple progradational geometry for the northwestern margin of the Friuli - Adriatic platform. Cuvillier et al. (1968) described for the first time the Cellina section and established the lithostratigraphy of the Platform. Ghetti (1987) better defined the slope units and described for the first time some around 30˚dipping clinoforms at the platform margin in the M. Cavallo group (Fig. 1). Costa et al. (1992) described the occurrence of mounds around 200 m wide and 50 m high in the Upper Cretaceous of the edge of the Friuli Platform, south of the M. Cavallo. Schindler and Conrad (1994) provided an important stratigraphic reconstruction of the margin of the Platform, measuring sections in the M. Cavallo group and dating the succession through a detailed biostratigraphy based on integration of benthic forams and Dasycladacean algae. Based on Schindler and Conrad (1994) work, in Fig. 2 it is possible to appreciate the margin stability between Berriasian and Aptian, with a slight progradation of around 500 m. The Albian is characterized by a backstepping trend of few hundreds of meters, possibly culminating in the earliest Cenomanian, whereas the most important change in the stratigraphic architecture occurred in the Cenomanian, when the clinoforms (talus facies in Fig. 2) established onto the underlying reef complex. This dramatic change is also visible in the changing lithostratigraphy, with the start of a new unit, the Calcareniti del Molassa (see Fig. 2).

So far, a comprehensive study on the stratigraphic architecture of the northwestern margin of the Friuli - Adriatic platform, linking the platform to the basin, is missing. With this contribution, we intend to bridge this gap, by integrating the previous knowledge and the new data into a coherent frame.

3. Methods and materials

In the Friuli Prealps, the Upper Jurassic to Cretaceous platform margin is well outcropping (Fig. 1), allowing to locate the chosen sections within a paleogeographic context. The CE section was located 8 km inside the margin, it measures around 1400 meters and is the most representative and best-studied sections of the Friuli- Adriatic Platform (e.g., Cuvillier et al., 1968; Ghetti, 1987;

Woodfine, 2002; Bernoulli, pers. comm.). According to the biostratigraphy of the quoted authors, refined by Bruni in Woodfine thesis work (2002), it encompasses the Upper Jurassic (Kimmeridgian) to the lowest Paleogene. In this paper, the literature data are summarised and integrated with new stratigraphical and sedimentological data, derived from original observations. The CE section was re-measured, taking advantage of the well signed benchmarks left by previous scholars, and 50 thin sections were studied for updating the microfacies. Standard XRD analysis on three clay interbeds was performed at ETH.

The CS section, already studied by Gnaccolini (1968) and Costacurta et al. (1979), was located at the base of slope, connecting the platform to the Belluno Basin, around 15 km off-margin. Based on new detailed sampling and measuring, we will describe its sedimentology and we analysed its foraminiferal (31 thin sections) and calcareous nannofossil content (52 samples), as well as the carbon and oxygen isotope composition of bulk carbonate (134 samples, 99 of them presented as supplementary material).

For the discussion on the local tectonic controls, we included two other stratigraphic sections (Fig. 1): the Istria composite section of Vlahović et al. (2005), presently located some 80 km southeast of the studied area, and the Puez section of Lukeneder (2010), located some 60 km to the northwest in the Trento Plateau (Fig. 1). Although this latter section is developed in a different paleogeographic domain, it has been chosen since it started depositing in the Upper Jurassic after a long-standing emersion, and rapidly evolved into an open sea plateau, therefore recording the subsidence in the studied interval.

3.1. Calcareous plankton

New biostratigraphy and age calibration of the CS section is based on calcareous nannofossils and planktic foraminifera. Fitfty-two samples were collected from marly interbeds and pelagic limestone for the calcareous nannofossil study. Calcareous nannofossils were analysed using simple smear slides and standard light-microscope techniques (Bown and Young, 1998). Nannofossil assemblages are quantitatively estimated, counting 300 specimens for each sample; abundance and preservation data are reported in the data repository. Biostratigraphy is described with reference to the biozonation of Roth, 1978 (NC zones revised by Bralower et al., 1995) integrated with Sissingh (1997) and Burnett (1998; Fig. 3). Twenty-seven samples were collected for their planktic foraminiferal content; biostratigraphy refers to the zonal schemes proposed by Coccioni and Premoli Silva (2015). Chronostratigraphic calibrations are according to Ogg and Hinnov (2012).

3.2. Bulk carbon and oxygen stable isotopes

Carbon and oxygen isotopic composition of the bulk carbonate was measured on 134 samples using a GasBench II coupled to a Delta V mass spectrometer (both ThermoFischer Scientific, Bremen, Germany) as described in Breitenbach and Bernasconi (2011). Briefly, about 100µg of powdered sample were placed in vacutainers, flushed with helium and were reacted with 5 drops of 104% phosphoric acid at 70ºC. In batch of 70 samples instrument was calibrated with the internal standards MS2 ($\delta^{13}C$ = +2.13 ‰, $d^{18}O$ = -1.81 ‰) and ETH-4 ($\delta^{13}C$ = -10.19 ‰, $d^{18}O$ = -18.71 ‰), which are calibrated to the international reference materials NBS 19 ($\delta^{13}C$ = +1.95‰, $d^{18}O$ = -2.2‰) and NBS 18 ($\delta^{13}C$ = -5.01‰, $d^{18}O$ = -23.00‰; Bernasconi et al., 2018). Values are reported in the conventional delta notation with respect to VPDB.

4. Results

We describe below lithostratigraphy, biostratigraphy, stable isotope data and results from CS. The stratigraphy of the CE section is synthetically described by integrating new observations and previous literature (Woodfine, 2002). Finally, the platform margin subsidence at CE is analysed in comparison to the composite sections of Istria (Vlahovič et al., 2005) and the measured section Puez (Lukeneder, 2010) (see Fig. 1). This allows us to evaluate the local factors controlling the main changes in the stratigraphic architecture and discuss them in the frame of global OAEs.

4.1. Casso section lithostratigraphy

The CS section (Fig. 4), 115 m thick, here described in its Aptian to Santonian interval, represents the base-of-slope succession where periplatform deposits are interbedded with normal to condensed pelagic, locally nodular, calcareous intervals. It is well exposed on the northern side of the Vajont valley, near the main road, in a cliff underneath the village of Casso (northeastern Italy), presently used as rock climbing wall. It has been measured starting from a hardground that separates the white porcellanaceous lime mudstones of the Maiolica (early to mid-Barremian in age) from the overlying grey and reddish limestone/marlstone couplets, thoroughly described by Costacurta et al. (1979).

The lowermost 9.7 m consist of thinly bedded grey cherty lime wackestone with radiolarian and planktic foraminifera, locally nodular at the base, interbedded with marlstones and black to red radiolarian chert layers. This succession tends to become reddish in the upper 5 meters, with upward increasing bioturbation. Towards the top (sample CSS 1), lime packstone contains pelagic bivalves, pelagic crinoids, *Inoceramus* remains, rare lagenids and lituolids and abundant planktic foraminifera. Separated by a downcutting erosional base, a 4.1 m thick massive greyish angular pebbly grainstone occurs. The matrix tends to become more micritic toward the top. The gravel sized clasts, coarser upward, consist of rudists and rudist-rich wacke- packstones, angular black and orange cherts and rounded lime wackestones, eroded from the underlying succession. In thin section, we observed fragments of rudists, corals and calcareous sponge, as well as orbitolinid foraminifera (*Conicorbitolina conica* and *Neoiraqia insolita*). Over this deposit, 2.8 m of medium bedded dark grey, nodular cherty lime wackestone occur, with thin to absent marly interbeds and rich planktic foraminifera fauna.

Floored by a sharp surface, 9.5 m of medium to thick bedded amalgamated lime grain/packstones follow. The microfacies is dominated by platform-derived clasts including rudists, peloids, echinids and benthic foraminifera, and very rare planktic forms. Shear planes are visible, rooted at the base of this interval, with clear compressional movement toward the west. The whole interval, therefore, is considered as a slumped mass, although the stratigraphy is preserved. This latter is covered by 3.15 m of reddish, slightly nodular and thinly bedded cherty lime packstone, rich of planktic foraminifera.

The following 14 m show a unique slumped mass involving two intervals. The lower 4 – 5 m consist of grey medium-bedded cherty lime wacke- packstone. The overlying interval consists of poorly and thick bedded lime grainstones, mostly formed by rudist fragments, micritized grains (pellettoids) and benthic foraminifera, including *Cuneolina parva*. The slump is formed by asymmetric folds, sheared limbs and unrooted hinges, showing a clear vergence towards the west. It is overlain by a 18-m-thick interval of light grey nodular limestones, passing upward to medium beds, consisting of thin amalgamated layers arranged in bundles of 30 – 40 cm, with black chert in nodules. In thin section, they are foraminifer and calcareous dinocyst rich lime wacke- packstone with evidences of bioturbation. With a sharp planar contact, a 3.15 m thick lime pebbly grainstone follows, showing inverse grading and water escape features. The sandy matrix, similar to the overlying grainstone beds (sample CSS 17), consists of a coarse mixture of rudist fragments, pelagic crinoids and peloids/pelletoids. The soft pebbles consist of lime wacke- packstones with *Pithonella* calcareous dynocysts, planktic foraminifera, rare benthic foraminifera and thin-shelled bivalves. This facies is very similar and probably correlates with the coeval Sveti Duh Fm, outcropping some 80 km to the southeast in Istria and Dalmatia (e.g. Brčić et al., 2017, see Fig. 1). Above, we identified a 18.8 m thick interval of alternating thin to medium bedded grey foraminifer-rich lime packestones with abundant medium to thick bedded greyish lime pack- to grainstones with white chert nodules. The grainstone beds show planar to cross lamination. The following 24 m consist of grey medium bedded lime wacke- packstones with dark chert nodules, interbedded with marls and alternating with thin layers of grainstones, locally laminated. The final 8.7 m consist of prevailing light grey lime grainstones, with planar to convolute lamination, in medium to thick beds with white chert nodules, alternating with thinner lime wackestones rich in planktic foraminifera and minor marly interlayers.

4.2 Casso section biostratigraphy

Considering the base-of-slope setting where the CS section was deposited, resedimented layers containing shallow-water fauna are interbedded with pelagic intervals, so that the presence of calcareous plankton is mostly restricted to the latter beds. The precise location of most zonal and stage boundaries is therefore prevented by the discontinuos occurrence of planktic assemblages and by hiatuses due to non-deposition and erosion at the base of coarser gravity-driven deposits. Nevertheless, the biostratigraphic analysis allows us to recontruct a complete chronological frame of the succession.

4.2.1 Calcareous nannofossils

A number of calcareous nannofossil bioevents are recognized through the CS (Fig. 4), according to the standard calcareous nannofossil biozonations (Fig. 3), even though nannofossil assemblages are heavily selected by diagenesis. Nannofossils are mainly rare, only the dissolution-resistant species are preserved and some stratigraphic intervals, characterized by nodular or massive limestones rich in pressure-solution structures, are completely barren.

The base of the section is characterized by the occurrence of *Rucinolithus irregularis*. At sample CS5, the first occurence of *Eprolithus floralis* is documented, whereas *Prediscopshaera columnata*, more dissolution susceptible, is recorded only in three samples: CS15, CS19 and CS26. It should be noted that the interval between CS12 and CS14 is affected by pressure solution seams and samples are often barren in calcareous nannofossils. The base of *Axopodorhabdus albianus* occurs from sample CS9; thus, its occurrence in sample CS9 points out that *P. columnata* should have been found at least before this event (Figs 3 and 4). The base of *Eiffellithus turriseiffelii* is noted in sample CS11. *Microrhabdus decoratus* is documented from sample CS18, but it becomes more frequent and continuously distributed from sample CS35 up to sample CS50. Again, the stratigraphic interval from CS16 to CS28 is mainly nodular and affected by frequent pressure-solution seams. In spite of that, the base of *Quadrum gartneri* occurs in sample CS21. This species is very rare and occurs only sporadically, therefore, some degree of uncertainty about the position of this event exists. The base of *Eiffellithus eximius* occurs in sample CS25; although rare, it is distributed continuously up to the section top. The base of *Micula staurophora* is recorded in sample CS29, after that it displays a continuous range. Although the relative abundances remain low, this marker displays a continuity in the range distribution probably due to the dissolution resistant behavior typical of the genus *Micula*. In sample C32 the base of *Lucianorhabdus cayeuxii* is found. From sample CS 35 to sample CS 37 it records an abundance acme. *Calculites obscurus* is observed from sample CS35. The base of *Broinsonia* sp. (cfr. *B. parca parca*) is recorded in the sample CS37.

Due to both the poor nannofossil preservation and the few biostratigraphic events recorded, the most useful biostratigraphic scheme to apply is Bralower et al. (1995), with some integration by Sissingh (1977) and Burnett (1998). The lowermost 4.5 m of the section is attributed to the NC6 Zone. Above, the interval from 4.5 m to 7.5 m is assigned to the indistinct NC7 and NC8 Zones, being the species *P. columnata* recorded after *A. albianus*. From 7.5 m to 14 m (LO of *E. turriseiffelii*), the section is ascribed to the NC9 zone. The upper boundary of the NC10 cannot be identified, due to the absence of *L. acutus*. The same holds for the NC11 to NC12 Zone boundary, being the top of *A. albianus* and *P. asper* not clearly identified in the studied samples. From 47 m to 82.5 m no markers used by Bralower et al. (1995) to define their zone's boundaries are recorded. On the contrary, the bases of *Quadrum gartneri* and *Eiffellithus eximius*, recorded in the section at 47 m and 61 m, respectively, were used by Sissingh (1977) to identify the lower and upper boundaries of the CC11 zone, which corresponds to the UC7 zone of Burnett (1998). The bases of *Micula staurophora* at 82.5 m and *Lucianorhabdus cayeuxii* at 90 m allow us to recognize the NC16 zone of Bralower et al. (1995). Above the interval from 90 m to 113 m is assigned to the NC 17 zone.

4.2.2 Planktic foraminifera

According to the planktic foraminiferal zonal schemes porposed by Coccioni and Premoli Silva (2015) the studied succession spans the *Pseudothalmanninella ticinensis* Zone to the *Dicarinella asymetrica* Zone. Planktic foraminifera are generally abundant enough and adequately preserved in the thin sections examined to provide the lateral views intersecting the proloculus, useful for species identification.

Pseudothalmanninella ticinensis Zone. This zone, that is the interval between the base of *Pseudothalmanninella ticinensis* and the base of *Parathalmanninella appenninica,* was identified in sample CSS1 that contains, besides the zonal marker, several ticinellids (e.g., *Ticinella primula*, *T. roberti, T. madecassiana)* in absence of *Parathalmanninella appenninica.* The presence of *Planomalina praebuxtorfi* refers the sample to the upper part of the zone.

Parathalmanninella appenninica Zone. Sample CSS6, that includes also echinoids fragments, contains a planktic foraminiferal assemblage typical of the *P. appenninica* Zone which is defined as the interval between the base of *Parathalmanninella appenninica* and the base of *Thalmanninella globotruncanoides*. The taxa recognized are: *Parathalmanninella appenninica, Heterohelix sp., Ticinella madecassiana, T. praeticinensis, T. primula, T. raynaudi, Planomalina buxtorfi* and *Biticinella breggiensis.* The occurrence of ticinellids and *B. breggiensis* refers this level to the lower-middle part of the zone.

Rotalipora cushmani Zone. Sample CSS7 contains rare planktic foraminifera. However, the occurrence of typical *R. cushmani* allows us to identify this total range zone. The species *Dicarinella algeriana, D. canaliculata* and *Whiteinella baltica* are also present.

Whiteinella archeocretacea Zone. Samples CSS8-CSS9 show a relatively rich planktic foraminiferal assemblages typical of the *W. archeocretacea* Zone. This interval is dominated by whiteinellids: *Whiteinella archaeocretacea, W. aprica, W. brittonensis, W. baltica* and *W. paradubia.* The species *Dicarinella algeriana, D. hagni, D. imbricata, Praegloboruncana gibba* also occur, in absence of rotaliporids and *Helvetoglobotruncana helvetica*, according to the zonal definition. The presence of *Whiteinella praehelvetica,* common in sample CSS9, indicates the upper part of the zone.

Dicarinella primitiva/Marginotruncana sigali (Marginotruncana schneegansi Auct.) Zone. This zone was identified in samples CSS12 to CSS16 due to the occurrence of common marginotruncanids (e.g., *M. coronata, M. renzi, M. sigali, M. schneegansi)* and dicarinellids (e.g., *D. canaliculata, D. hagni*) in absence of *Helvetoglobotrunaca helvetica* and *Dicarinella concavata,* according to the zonal definition.

Dicarinella concavata Zone. The occurence in the planktic foraminiferal assemblage, dominated by marginotruncanids, of the zonal marker, in absence of *Dicarinella asymetrica,* allows us the identification of this zone in sample CSS19.

Dicarinella asymetrica Zone. This total range zone was recognized from sample CSS20 up to the top of the section due to the presence of the zonal marker. The planktic foraminiferal assemblages include also marginotruncanids, *Globotruncana linneiana*, *G. stuartiformis* and *Sigalia* sp.

4.2.3 Integrated calcareous plankton stratigraphy

The correlation between the main calcareous nannofossil and planktic foraminiferal biostratigraphic events and biozones is indicated in Fig. 4. As mentioned before, the two fossil groups investigated are not evenly distributed throughout the section. Nevertheless, we are able to highlight analogies and differences with the previous schemes of Bralower et al. (1995), Sissingh (1977), Burnett (1998) and Coccioni and Premoli Silva (2015), as it can be better appreciated by a comparison with Fig. 3.

At least the stratigraphic interval ranging from 6 to 9.7 meters from the bottom is assigned to the foraminiferal *Pseudothalmanninella ticinensis* Zone, which correlates with the upper part of the nannofossil NC8 and lower part of the NC9 zones of Bralower et al. (1995), corresponding to the CC8 zone of Sissingh (1977). Above, the foraminiferal *Parathalmanninella appenninica* Zone is identified: the correlation of this interval with the nannofossil NC10 Zone of Bralower et al. (1995) testifies that only the upper part of the *Parathalmanninella appenninica* Zone is preserved (Figs. 2 and 3). The lower slumped calcarenite is attributed to the upper part of the foraminiferal *Rotalipora cushmani* Zone. This biozone in the CS section correlates with the lower part of a long interval, which includes the nannofossil NC10-NC12 combined zones corresponding to the CC9-CC10 zones interval. The *Whiteinella archeocretacea* Zone (from 26.1 to 29.25 m) correlates with the long stratigraphic interval corresponding to the NC10-NC12 (CC 9-CC10) Zones. It is worth pointing out however that the *Helvetoglobotruncana helvetica* Zone was not detected in the CS. Above the upper slumped interval (Fig. 4), the *Dicarinella primitiva/Marginotruncana sigali (Marginotruncana schneegansi Auct.)* Zone can be identified from 43 to 67.5 m, even though we are not able to precisely locate the boundaries. Here there is a strong correlation problem with the nannofossil biozones because the observed first occurrences of *Q. gartneri* and *E. eximius* are probably younger than their FADs. For this reason, the CC11 Zone of Sissingh (1977) corresponding to Burnett's (1998) UC 7 that should correlate the *H. helvetica* Zone, correlates in this case with the overlying *Dicarinella primitiva/Marginotruncana sigali* Zone.

The interval from the base of *E. eximius* to the base of *M. staurophora* (22 m thick) is within the long range NC13-NC15 combined Zones (UC 8-10) which correlates the upper part of the *Dicarinella primitiva/Marginotruncana sigali* Zone and the lower part of the *Dicarinella concavata* Zone. Above, the nannofossil NC16 of Bralower et al. (1995) (CC14-15 of Sissingh, 1977) falls at the transition between the *D. concavata* and *D. asymetrica* Zones. Finally, the NC17 Zone (CC16 and CC17) correlates the *D. asymetrica* Zone.

The correlation between planktic foraminiferal and calcareous nannofossil zones, except for the above-mentioned interval, is consistent with the schemes previously proposed.

4.3 Carbon isotope data

In the CS section, the measured bulk $\delta^{13}C$ values span from a maximum of +4.0‰ in the Aptian to a minimum of +2.1‰ VPDB in the lower Santonian (Fig. 4). In the lower 10 meters of the section, the $\delta^{13}C$ curve shows a very distinctive shape. The largest shift of +1.6‰ is measured in this part, with a maximum of 4.0‰ at 4 m. After this positive peak, an interval from 8 to 17.5 m showing lower $\delta^{13}C$ values is recorded. One positive shift is identified in the middle part of this depression (12.5 m from the bottom section). Above, another distinctive large positive excursion, from 17 to 30 m, is detected with values between 3.2‰ and 3.5‰.

The slump deposits have not been sampled for isotope analysis. In the overlying stratigraphic interval, two distinctive negative shifts are observed, respectively at 47.5 m and 52.5 meters, with a positive excursion in between. The minimum $\delta^{13}C$ value in this part is in the upper negative peak of 2.13‰.

The characteristic features in the stratigraphic interval above are the general increase in the $\delta^{13}C$ values from 2.13‰ at 52.5 m to 3.15‰ at 71 m, and the following decrease trend to 2.12‰ at 92 m. From 92 to 110 m, the $\delta^{13}C$ values are relatively stable between 2.12‰ and 2.25‰ with weak increasing and decreasing trends. In the upper part of the section, the $\delta^{13}C$ values show a very characteristic increase up to 3.0 ‰ at 115 m.

4.4 Val Cellina section litho- and biostratigraphy

The CE section has been described in several papers, including Cuvillier et al. (1968), Ghetti (1987) and Woodfine (2002). This latter author, thanks to the collaboration with R. Bruni (in Woodfine, 2002), revised the biostratigraphy, based on dasycladacean algae and benthic foraminifera, and measured the C, O and Sr isotopes. These latter allowed the author to confirm the results of the biostratigraphy. In this paper, we performed a new biostratigraphic analysis, and adopted the revised biostratigraphic scheme of Chiocchini et al. (2008). Our results have been integrated with those of the previous authors, especially Woodfine (2002), and are shown in Fig. 5, where we report the most diagnostic forms. For the Lower Cretaceous, we compared our data with the results from Schindler and Conrad (1994) (Fig. 2), who analysed similar successions around 8 km to the west, at the platform margin. Between the two sections (Cellina and M. Cavallo), the thickness of the various time intervals is in good agreement (Figs 2 and 5).

The lower lithostratigraphic unit of this section is a 1025 m thick peritidal succession, known as Calcare del Cellina (Cuvillier et al., 1968), encompassing the Upper Jurassic (?Oxfordian) to the very base of the Upper Cretaceous (lower Cenomanian). It consists of a monotonous stacking of tidal cycles including subtidal peloidal lime pack- grainstone, often rich in green algae and benthic foraminifera. Less developed are the inter/supratidal divisions, locally with planar stromatolites or aligned fenestrae. Bedding is thick to massive and coarse grainstones are interbedded especially in the lower 200 m (see Fig. 5). A unit of medium-, locally thin-bedded micritic limestones occurs between 240 and 305 m. This interval is poor in fossils, and it contains an oligotypic ostracod fauna indicating brackish water conditions. It correlates with an interval of similar age found by Schindler and Conrad (1994, their pond facies) at the platform margin, around 8 km to the west. We confirm the base of the Cretaceous at around 300 m thanks to the first occurrence of *Actinoporella podolica* immediately above the brackish water facies (Fig. 5). The interval between 341 and 370 m is characterized by the occurence of cm-thick green claystone cap topping most of the tidal cycles. The same feature is recorded in the upper Barremian to lower Aptian, between 768 and 812 m (see also Woodfine, 2002). We analysed these clays by XRD and found that they consist of a mixture of illite, kaolinite and vermiculite, with minor chlorite. The base of the Hauterivian has been tentatively placed at 495 m, owing to the occurrence of the first *Cuneolina sp*., followed by *Prechrysalidina infracretacea*. This succession of events was used by Schindler and Conrad (1994) and Chiocchini et al. (2008) for the characterization of the Hauterivian. Between 730 and 760 m, the bedding is disturbed by soft sediment deformation, associated with two opposite dipping normal faults with a NE trend. The Aptian interval, between around 780 and 875 m is indicated by the co-occurrence of *Salpingoporella dinarica* and *Palorbitolina lenticularis*, species reaching their acme in the early Aptian (e.g. Chiocchini et al., 2008). The Albian is well documented in its upper part, owing to the presence of *Neoiraqia convexa, Cuneolina parva* and *Dyctioconus algerianus*., but especially thanks to the presence of the planktonic foraminifer *Pa. appenninica*. The Albian – Cenomanian transition is peculiar, since we have some planktonic foraminifera typical of the late Albian (sample CE BE, after Ghetti, 1987) at around 980 m, followed by the benthic foraminifera at 995 m defining the upper Cenomanian biozone of Chiocchini et al. (2008). This would suggest the lower Cenomanian is reduced or even missing.

The overlying unit, named Calcareniti del Molassa by Ghetti (1987), clearly differs from the underlying interval due to its massive banks and the peculiar geometries. The grain size is much coarser, rudist fragments occur in coarse rudstones - grainstones, with locally abundant benthic foraminifera. The most peculiar facies, not recognized by the previous authors, are the organic buildups, showing elevations of 25 to 35 m and basal diameters of around 50-70 m, visible between 1148 and 1350 m in the section (Figs. 4 and 5). The microfacies of these coalescent mounds shows widespread evidence of microbial activity, such as *Lithocodium-Bacinella* boundstones (Fig. 6c, with abundant fragments of rudists and benthic foraminifera and encrusting micrite (i.e. automicrite) that shows thrombolite and leiolite textures. The steep mounds flanks, around 25-30˚ (Fig. 6a and 6b) document a very early diagenesis, and their elevation was likely controlled by the storm waves. Whole specimens of rudists characterize the mounds, whereas only rudist debris charachterized the intra-mound depressions. These *Lithocodium-Bacinella* buildups are common in the Lower Cretaceous of the southern Tethys, and they have been associated to paleoenvironmental perturbations on the shallow water carbonates (mostly around the Aptian OAE 1a, e.g. Rameil et al., 2010).

The base of Turonian is placed at around 1250 m, at the first occurrence of *Pseudolituenella reicheli, Chrysalidina gradata* and *Dyciclina schlumbergeri* (Bruni, in Woodfine, 2002). A more recent work (Frijia et al., 2015) considers the first two forms still Cenomanian, and the third Coniacian. The isotope curve of Woodfine shows a positive peak at around 1280 that could be correlated with the top Cenomanian excursion. If this is true, then the Cenomanian - Turonian boundary at CE should be shifted up by around 30 m. The final 58 m of this unit consists of structureless massive rudstones in thick banks, again dominated by rudists debris, and showing fossils typical of the Coniacian – Santonian (*Accordiella conica* at 1350 to 1375 m) and Campanian – Maastrichtian (*Orbitoides tissoti*, *G. stuarti*), up to 1408 m. Another peculiarity of the Upper Cretaceous unit is the occurrence of planktic foraminifera, actually found already at the top of the Calcari del Cellina at around 980 m. They are found in scattered positions within the column, but they could be determined only in sample CE 19B, where they confirm the age based on benthic foraminifera. The Cretaceous platform ends with an unconformity, marked by few centimeters of a yellowish grainstone including reworked rudist, Paleocene planktic foraminifera and fish teeth, and the overlying Thanetian platform (Cuvillier et al., 1968) consists of corals, red algae and nummulitids.

4.5 Subsidence history of the northwestern margin of the Friuli-Adriatic Platform

In order to unravel the local factors controlling the main changes in the stratigraphic architecture, we analysed the subsidence pattern of the platform margin at the CE section and compared it with the composite section “Istria”, taken from Vlahovič et al. (2005), and with the Puez section (Lukeneder, 2010). This latter section crops out in the Dolomites on a different paleogeographic domain, the northern Trento Plateau, an area that remained subaerially exposed from the end of the Triassic until the Late Jurassic (e.g. Masetti et al., 2012). Late Jurassic in age is also the oldest unit outcropping at the CE section (Fig. 6).

The subsidence curves for Cellina and Istria have not been corrected for compaction or water depth, since they were continuously deposited in peritidal to upper neritic environment and they underwent early diagenesis and lithification prior to the deep burial. Features in outcrop and thin sections document this early diagenesis, with absent grain boundary pressure solution contacts and very limited bed parallel solution seams. Given the temporal scale involved in our study, in the order of around 100 My, also the sediment load component has not been considered, and the sediment accumulation is shown to represent the total tectonic subsidence. In the case of Puez section, the water depth of this pelagic, ammonite-rich section could not be well established, however, the unit starts from the prominent subaerial unconformity with around 3 m of dolosparitic carbonates, very likely representing shallow-water conditions, approximately 20 to 60 m. These latter dolostones are followed by an Upper Jurassic to Lower Cretaceous deepening upward succession (Lukeneder, 2010). Since the paleobathymetry of this succession is unknown, the curve of the Puez section does not represent the total tectonic subsidence (Fig. 7), but only the sediment accumulation. It has been drawn with a different scale in order to compare the timing of the major changes with those of the CE and Istria.

The subsidence in the Friuli-Adriatic Platform at CE section starts at quite high rates in the Late Jurassic (around 30 m/Myr, Fig. 7), and then it decreases to around 7 m/Myr at the onset of the Cretaceous. The Hauterivian to Barremian subsidence curve records a sharp increase, up to 44 m/Ma, followed by a deceleration in the Aptian to Albian, with values again in the order of few meters/Ma. The late Cenomanian shows the highest subsidence rate (near 70 m/Myr), followed by a gradually decreasing trend during the Turonian, but strongly decelerating at Coniacian to Maastrichtian. After a gap encompassing the early Paleocene, the subsidence resumed with around 10 m/Myr up to the end of the measured section.

The Istria section displays different Late Jurassic subsidence history, but the overall pattern is similar to CE, with a slight subsidence increase at the Hauterivian to Barremian transition, low rates in the Aptian to mid-Albian and a sharp increase up to 78 m/Myr throughout the mid Albian to Santonian. The Campanian, Maastrichtian and early Paleocene are not represented in the Istria section, whereas the sediments record a late Paleocene to Eocene recovery of subsidence (Fig. 7).

The Puez section starts with a Late Jurassic pulse of subsidence, not better defined, owing to the lack of paleobathymetric indications, that was tentatively assessed at the end Jurassic as 40±20 m, i.e. lower than the wave base, in a pelagic setting. However, the uncertainties could be much higher, therefore we will describe only the sediment accumulation rates for a comparison with the tectonic subsidence given on the Friuli-Adriatic platform. The pattern of sediment accumulation in the Puez section is very similar to the two platform sections, with an increase in the Hauterivian to Barremian interval, a sharp decrease during the Aptian, and the abrupt increase during the Albian to Cenomanian, until the end of the measured section.

Overall, it is worth noting the three sections share a similar Hauterivian to Barremian pulse of subsidence/sediment accumulation, whereas the next pulse is older in the northwest, at Puez (Albian) and younger in the southeast, at CE (Cenomanian). Istria shows an intermediate behaviour, starting the new pulse at mid Albian. The Albian to Cenomanian is a time of major changes in the architecture of the northwest Friuli-Adriatic Platform. Until the Albian, in fact, the whole domain was dominated by a large subsiding carbonate platform, whereas afterwards the sedimentation focused only in some areas to the north and east, with progressive important subsidence and the rest of the platform emerged. The post-Albian coastal onlap, hinge between emerging and subsiding Platform, can be traced, based on surface and well data, as it is shown in Fig. 1.

5. Bio- and carbon isotope stratigraphy and record of global carbon cycle perturbations in the Casso section

The $\delta^{13}C$ curve here provided for the CS section is calibrated with calcareous nannofossil and planktic foraminiferal biostratigraphy and allows us a comparison with other Cretaceous curves (e.g., Weissert et al., 1998; Stoll and Schrag, 2000; Jarvis et al., 2006; Sprovieri et al., 2013; Thibault et al., 2016). This comparison is however rather difficult for some intervals due to the occurrence of gaps and condensations in the CS section. Furthermore, the scarce preservation of nannofossil assemblages within the micritic limestones, prevents in some cases an accurate biostratigraphy. In spite of that, we succeeded, based on our revised biostratigraphy, in recognizing and correlating several major C-isotope shifts.

5.1 The Aptian- Cenomanian $\delta^{13}C$ *events*

At the base of the section, a positive carbon isotope excursion occurs (Fig. 8A). It is the most prominent of the entire CS curve (from 2.42‰ to 4.04‰) and falls immediately below the first occurrence of *Eprolithus floralis*, which defines the lower boundary of the nannofossil NC7 zone. The stratigraphic position of this peak is compatible with the globally recognized positive carbon excursion that follows a negative peak, related to the Oceanic Anoxic Event 1a (Menegatti et al., 1998). In particular, our $\delta^{13}C$ values are comparable with those recorded by Weissert et al. (1998) in other Italian Tethyan sections, Cismon and Piobbico (Fig.7A). Most of the upper Aptian, lower and middle Albian is not preserved in our section, probably due to condensation and an erosional gap below the slump breccia. Therefore, our $\delta^{13}C$ curve does not contain the negative shifts related to the OAE1b. A minor positive peak (Fig. 8B, values from 2.3 to 2.9‰) is recorded at 11 m in the pelagic matrix of the breccia body and is considered as of late Albian age (Zone NC10 and *Pa. appenninica* Zone). This peak has a possible analogy to the English chalk carbon stable isotope values of Jarvis et al. (2006), representing the OAE 1d. OAE 1d is a short positive $\delta^{13}C$ excursion in the range of 1.7-2.3‰ (Jarvis et al. et al., 2006), below the Albian-Cenomanian boundary event. Above it, the erosive nature of the calcarenite bed and the occurrence at its top of foraminiferal assemblage of late Cenomanian age (*Rotalipora cushmani* Zone) suggest that large part of the lower to middle Cenomanian interval is missing, as also highlighted by Costacurta et al. (1979). In the late

Cenomanian *Rotalipora cushmanii* Zone, found within the calcarenite bed, a clear and broad positive $\delta^{13}C$ interval, with values over 3‰ (Fig. 8), is recorded. This positive excursion, found also on other margins of the AdCP (Davey and Jenkyns, 1999), can be correlated with Oceanic Anoxic Event 2 interval. According to different authors (Jarvis et al., 2011; Gambacorta et al., 2015; Jenkyns et al., 2017) the OAE 2 isotopic event spans from the initial level of positive excursion in $\delta^{13}C$ to the point of the definitive carbon isotope drop that falls into the base of Turonian. In the CS section (Fig. 8), the foraminiferal assemblages recorded above this peak belong to the *Whiteinella archaeocretacea* Zone, which spans the topmost Cenomanian and the lower Turonian. Therefore, we can assume that this peak represents the Cenomanian/Turonian Boundary Event (CTBE). It is worth noting that the black shales of the Selli and Bonarelli Levels, the sedimentary expression of the Oceanic Anoxic Event 1a and 2 in basinal successions of the western Tethys (e.g. Schlanger and Jenkyns, 1976; Giorgioni *et al*., 2015), do not occur in the CS section. In the slope setting of the CS section, these perturbations of the carbon cycle are only recorded in the $\delta^{13}C$ curve.

5.2 The Turonian $\delta^{13}C$ events

Between 45 to 80 m of the CS section, four chemostratigraphic events have been found and match the events recorded at Culver Cliff (Isle of Wight) and Dover (Kent) (Jarvis et al., 2006) (Figs. 8 and 9). The lower event is a positive peak of the CS $\delta^{13}C$ curve (2.5-2.8‰; Fig. 9) that correlates the Caburn event (Jarvis et al., 2006). This correlation is well costrained by its biostratigraphic position within the middle Turonian *Dicarinella primitiva/Marginotruncana sigali* Zone. The two intervals of low values below and above this peak in our section further support the correspondence with the Caburn event (Fig. 9). Specifically, the small negative $\delta^{13}C$ excursion with a minimum value of 2.1‰ (peak 5) that occurs above the Caburn peak can be attributed to the Bridgewick event (Jarvis et al., 2006). The peak at 73 m, following the long positive trend, is tentatively assigned to the Hitch Wood event (Jarvis et al., 2006). The position of this peak in the CS section within the *Dicarinella primitiva/Marginotruncana sigali* Zone agrees with the biostratigraphic position of the Hitch Wood event (Jarvis et al., 2006). Furthermore, the base of *Eiffellithus eximius* occurs below the Hitch Wood event, as recorded in the reference curve, although its stratigraphic position could be biased by the underlying occurrence of nodular limestones, nannofossil barren. Across the Turonian/Coniacian boundary, a clear decrease in the $\delta^{13}C$ values of nearly 1‰ has been labelled as the Navigation event in the Jarvis et al. (2006) curve and it falls at the base of the *Dicarinella concavata* Zone. The negative $\delta^{13}C$ excursion shift in the CS section (- 0.5 ‰) recorded at 80 m, is less pronounced, but its position within the same planktic foraminiferal zone suggests that it might represent the Turonian/Coniacian Boundary Event.

5.3 The Coniacian-Santonian $\delta^{13}C$ events

In Fig. 10, the Coniacian - Santonian chemostratigraphy of the CS section is compared with the reference curves of Jarvis et al. (2006), Sprovieri et al. (2013) and Thibault et al., (2016). The low resolution of this part of the CS section, however, prevents a correlation based on individual peaks, therefore we compared and highlighted the general trends of the δ^{13}C curve and the recorded maximum and minimum values (Fig. 10). The Coniacian δ^{13}C curve of the CS section begins with a rise of values from around 2.5‰ up to 2.9‰ at the turning point, indicated in Fig. 10 as E_1. The curve proposed in the study of Jarvis et al. (2006) matches our curve quite well, showing the same general trend that is highlighted in light blue colour. Moreover, the values of the δ^{13}C shifts in both profiles are nearly the same (2.9‰). The lower to mid-Coniacian age of the Coniacian peak is recognized by its occurrence within the lower part of the nannofossil Zone NC16 (Bralower et al., 1995), which agrees with the reference curve (Jarvis et al., 2006) (E in Fig. 10). Above this peak, a marked negative trend of around - 0.8‰ to a minimum of ca 2.1‰ occurs in the upper Coniacian (from E_1 to F_1). A similar negative trend from around 2.7‰ to 2.0 ‰ is recorded in the English Chalk (from E to F). Furthermore, the Coniacian/Santonian Boundary Event has been correlated with the tightly coupled negative and positive shift in the English Chalk (Jarvis et al., 2006; F-G-H in Fig. 10). In the central Italian Bottaccione section, Sprovieri et al. (2013) further documented a positive shift occurring between the first occurrence of the *Micula staurophora* and the first occurrence of *L. cayeuxi*, that define the Zone NC16. Therefore, in the CS section, the negative shift with values of +2.2‰ at 94 m followed by slight positive peak could correlate the Coniacian/Santonian-Boundary Event (CSBE) and indicated as F_1 in Fig. 9. Finally, the positive peak K_1 (Fig. 10) could correspond to the chemostratigraphic Santonian/Campanian boundary of Jarvis et al. (2006) (Fig. 10). At the top of the section, the first occurrence of *Broinsonia* sp. (cfr. *B. parca parca*), which define the base of the Zone NC18 (Bralower et al., 1995), is recorded immediately above the chemostratigraphic Santonian/Campanian boundary, as documented also by Sprovieri et al. (2013) and Thibault et al., (2016).

6 Change from rimmed to ramp geometry

6.1 Regional tectonics

During Hauterivian to Barremian, the northwest Friuli-Adriatic Platform and the surrounding domains of the Adria plate were affected by extensional tectonics, creating the surface faulting that interfered with sedimentation in the CE section (see Fig. 11). This extensional event, in the literature described for the adjacent Belluno Basin by Doglioni (1992), is the responsible for the coeval subsidence pulse visible in Fig. 7, and affecting mostly the CE and perhaps the Puez sections. It is therefore unclear if this change in subsidence is of local or regional importance. One may argue that changes in subsidence of the proximal continental margin of Adria were associated with changes in plate movement, as paleomagnetic data document the onset of counterclockwise rotation of Adria starting in the Early Cretaceous (e.g. de Leeuw et al., 2012). Anyhow, this event did not change the paleoenvironmental conditions on the platform which remained stable and productive throughout the time of interest in this study (see Fig. 11).

However, Albian to Cenomanian tectonics deeply changed the stratigraphic architecture of the platform margin (e.g. Otoničar, 2007). The Friuli-Adriatic Platform was tilted north- and eastward and the sedimentation on its southern and western part definitively stopped with final emersion (see the location of the coastal onlap in Fig. 1). The transition from Albian to Cenomanian in the CE section recorded first an open-sea influence, as documented by the findings of upper Albian planktic foraminifera. This change was followed by an abrupt pulse of subsidence reflected in the thick Cenomanian. At the same time, (?normal) faulting was active also at the base-of-slope, as documented by the creation of new intrabasinal highs, rich in fish remains and devoid of periplatform resediments (Castellavazzo high, Fig. 11; Bassani, 1886). We relate these movements to the propagation of a foreland ramp. The final position of the bulge was located to the south of val Cellina, as it is demonstrated by the location of the coastal onlap (Fig.1). This Cretaceous foreland situation of the Friuli platform was never highlighted in the eastern Southern Alps, whereas it has been clearly documented in the western Southern Alps, where it is related to the development of the so-called Lombardian Flysch basin (e.g. Bersezio and Fornaciari, 1994; Bertotti et al., 1998; Zanchetta et al., 2015). The composite section “Istria” shows an intermediate behaviour, with a late Albian increase in subsidence (Fig. 7). More detailed data from this region (e.g. Tišljar et al., 1998; Otoničar, 2007) indicate that the flexural subsidence was creating a westward prograding subsidence pulse, with final flexure toward the east (Gušić and Jelaska, 1993; Brčić et al., 2017).

Overall, the three chosen sections for the subsidence analysis indicate a progressive integration into the Alpine/Dinaric foreland between the Albian and the Cenomanian (Fig. 7). The shape of the reconstructed coastal onlap (Fig. 1), turning from E- into S- oriented, documents that the northwestern Adria plate was already flexed toward the Alps to the North and the Dinarides to the East. We suspect that this corner represented the transition from a pro-foreland basin with respect to the Dinarides to a retro-foreland basin with respect to the Alps. However, no remnants of Cenomanian foreland basins to the north of the study area occur, therefore we cannot test this hypothesis.

6.2 Changes on the Friuli-AdCP margins as a response to mid-Cretaceous paleooceanographic events

Our integrated stratigraphy allows us to evaluate the impact of the mid-Cretaceous paleoceanographic events on the portion of the studied Friuli-Adriatic platform margin, considering its tectonic history. At the northwestern rim of the Friuli-Adriatic platform, the platform was aggrading during the whole Late Jurassic and Early Cretaceous and the margin remained stable and productive, with progradation/retrogradation of few hundreds of meters only (Schindler and Conrad, 1994). Adopting the inferred end-Aptian paleobathymetry of around 1500 m for the Belluno Basin (Picotti and Cobianchi, 2017), the slope dip should have been on average 5°, although the upper slope could have been locally much steeper, and the lower much less. This was a starving slope (Picotti and Cobianchi, 2017), likely due to the local oceanographic conditions, such as the prevailing currents/winds that were interacting with the rigid reef marginal frame to hinder offshore sediment transport. The transition from a rimmed platform to a ramp occurred abruptly at the end of the Albian. At the base-of-slope (CS), this event is expressed by the upper Albian mud-supported breccia, containing some calcareous sponges and corals, as well as rudists, and interpreted as the product of the collapse, perhaps tectonically induced, of the oversteepened margin at the transition from an accreting to a bypass/erosional slope (see Figs 2 and 11). This bioconstructed margin never recovered afterward. After the significant decrease of subsidence (CE) and a corresponding decrease in sedimentation (CS) in the early Cenomanian, the upper Cenomanian base-of-slope records the first resedimented sand bodies (CS). The arrival of the sands documents the important change in sediment production of the platform, whose absent margins allowed the formation of mobile sand shoals and the start of sediment export towards the basin, reaching the slope as grain flows, likely during major storms or earthquakes. These changes have been reported for other margins in the western Tethys by Carannante et al. (1997), who suggested a role of environmentally stressed foramol communities. The post-Albian CE section represented the middle-upper part of this ramp (Fig. 11), an environment that allowed a better connection to the lower slope. The occurence of clinoforms around 30-40 m high (Ghetti, 1987) at the distal part of the ramp, overlying the previous back-margin (Fig. 2; Schindler and Conrad, 1994) indicates the steepening of the former margin and the creation of a distally-steepened ramp. Mounds of 50 m in elevation characterize the external part of the ramp (Costa et al., 1992), compared to the 25-30 m mounds of the Cellina section. Their elevation documents the high accommodation space, increasing northwestward, due to a combination of abruptly increased subsidence (see Fig. 7 and 11) and high sea-level (e.g. Giorgioni et al., 2015).

Why did the platform change its geometry so abruptly at the end of the Albian? The platform experienced previous abrupt subsidence pulses already during Hauterivian to Barremian (see Figs. 6 and 10), without any modification in the platform geometry or the carbonate factory. In the studied platform, OAE 1a to 1c (early Aptian to Albian) did not affect the carbonate factory nor the margin geometry, as documented by the persistence of marginal reef (Schindler and Conrad, 1994). Other parts of the AdCP were more affected by these first Cretaceous OAE's, with local decrease to interruption of the carbonate productivity, but always recovering after the crisis (e.g. Huck et al., 2010; Cvetko Tesović et al., 2011; Husinec and Read, 2018). One example of a partially drowned margins of a different southern Tethyan platform during the OAE 1a is the east Apulian margin at Gargano, as described by Bosellini et al. (1999) and Luciani et al. (2006). The OAE 2 (latest Cenomanian) in the AdCP was more effective in decreasing the carbonate productivity, with drowned intervals persisting for most of the Turonian, like the Sveti Duh Fm (e.g. Jenkyns, 1991; Korbar et al., 2012; Brčić et al., 2017).

More generally, in the southern Tethyan platforms, these oceanic events never caused final drowning of the carbonate platforms that only show a decreased productivity and some paleoecological changes (e.g. *Orbitolina* level, Cherchi and Schroeder, 2013; Amodio and Weissert, 2017; *Lithocodium-Bacinella* intervals, Huck et al., 2010; stepwise extinction of large benthic foraminifera, Parente et al., 2008). Southern Tethys isolated carbonate platforms of Cretaceous age were less sensitive to environmental perturbations than the northern Tethyan carbonate platforms and ramps (e.g. Huck et al., 2010; Amodio and Weissert, 2017). This fact was considered paradoxical by Huck et al. (2010), given the high temperatures of the oceans during OAE's. A possible explanation was provided by Skelton and Gili (2012), who proposed the so-called "kettle effect", i.e the degassing of excess CO_2 in shallow and hot ocean waters, allowing the carbonate productivity. The AdCP was one of the largest isolated banks in the southern Tethys (e.g. Vlahovič et al., 2005), where the carbonate productivity could have benefited from this effect. Another possible explanation could be the different original profile of the carbonate platforms, more frequently rimmed in the southern Tethys for the presence of the tropical factory. Rimmed platform margins could have sheltered the oxygen depleted waters forming on the expanded oxygen minimum zone, whereas ramps, more frequent in the northern Tethys, were likely more vulnerable to them. Recent work on the AdCP (Hueter et al., in review), however, suggest the oxygen-depleted waters forming during the OAE 1a could encroach at least parts of the lagoon, bringing about the temporal disappearence of rudists in favour of the microencruster *Lithocodium-Bacinella*.

In the Friuli platform at the Cellina section, the only evidence for open sea influence that could be seen as an incipient drowning occurred in the late Albian, is the presence of levels with planktic foraminifera in the upper Albian shallow water succession (see Fig. 5). The Cenomanian platform recorded a change not only in geometry, but even in the main component of the carbonate factory that records the disappearance of hermatypic corals and calcareous sponges and their substitution by microbial mounds and rudists. In the study area, these changes appear coeval with the OAE 1d (late Albian, see Fig. 11), related to the first important lava flows in the late Albian Ontong Java 2 system (Kidder and Worsley, 2010). We do not claim that this climatic perturbation was stronger than others eventually leading to OAEs, rather we think that the carbonate platforms in the southern Tethys were affected by repeated perturbations that collectively created less favourable conditions for the tropical factory (e.g. Hallock 2001), eventually culminating, for the studied Friuli Platform, in the late Albian. This change occurred slightly before the subsidence pulse related to the incipient flexuring of the Alpine - Dinaric foreland (Fig. 7).

The post-Albian oceanographic conditions allowed for a shift of the focus in carbonate sedimentation from shallow- to deep-water settings, by favouring on one hand the proliferation of the rudists, thanks to the increasing current activity sweeping the shelf and enhancing the particle distribution (e.g. Carannante et al., 1997), and on the other hand the bloom of the microbes, especially the encrusting *Lithocodium-Bacinella* that is so widespread in the Tethys particularly during the mid-Cretaceous, where they have been described in mid- upper ramp settings (e.g. Rameil et al., 2010). These conditions, however, occurred locally at the studied northwest corner of the larger AdCP. In fact, toward the east in Istria and south of it (see Fig. 1), the east-dipping Cenomanian ramp was characterized by partial drowning, with pelagic limestones rich in open-sea organisms (Gušić and Jelaska, 1993; Korbar et al., 2012; Brčić et al., 2017). These facies, started around the early-middle Cenomanian, reached the maximum diffusion at the Cenomanian/Turonian boundary, which may be seen as the effect of OAE 2 and related sea-level rise on the platform margin.

7 Conclusions

Detailed stratigraphy of the two Val Cellina and Casso sections, located at the northwestern Friuli-Adriatic Platform and its slope, respectively, and the reappraisal of the available stratigraphy from the literature, allowed us to reconstruct the major changes in the sedimentary architecture which occurred throughout the mid- Cretaceous, a time of plate reorganization and global climatic and paleooceanographic changes.

A major change in the platform geometry, from a rimmed platform bordered by a steep slope to a distally steepened ramp, had profound effects on its capability of offshore sediment export, therefore ending a starvation phase at the base of slope. This change occurred during the late

Albian, and it is controlled by the co-occurrence of local tectonics and events affecting global climate and paleooceanography.

Deformations related to the foreland of the Alps and the Dinarides progressively encroached the former passive margin. Starting from the north in the Albian (Trento plateau), the pulse of subsidence associated with the northward flexure arrived in the study area during the Cenomanian. Coeval emersion in the south of the Friuli Platform defined a wedge of platform deposits and contributed creating the ramp geometry at the platform margin. As visible from the trend of the coastal onlap, the geometry of the flexure was conditioned since the Cenomanian by the interference with the Dinarides, with a sharp turn to the east of the flexed Adriatic crust northwest of Trieste. One first outcome from this interference geometry is that the northwestern Friuli-Adriatic Platform acted since the Late Cretaceous as the common foreland for the Alps (retroforeland) and the Dinarides (proforeland).

The studied Carbonate Platform, isolated and located at low latitudes, was less sensitive to the mid-Cretaceous OAEs, very likely due to the "kettle effect". However, the cumulative effects of the OAEs stressed also the carbonate factory of these resilient southern Tethyan Platforms. At the northwest Friuli- AdCP, the threshold for the disappeareance of the delicate ecosystem of hermatypic corals and calcareous sponges was abruptly exceeded around the OAE 1d (late Albian), with the recorded transition toward a ramp setting progressively dominated by rudist- *Lithocodium-Bacinella* mounds. The disappeareance of the frame builders impacted the stratigraphic architecture of the whole platform that was shaped as a ramp thanks to the concurrent northward tectonic tilt with emergence of the southermost areas (see Fig. 11). The rise of the chemocline, associated with increased sea-level and vertical mixing, likely pushed less oxygenated water towards the platform margins, that contributed to the observed late Albian to Turonian partial drownings and rimmed to ramp change in the platform architecture.

Acknowledgments

The Authors are grateful to Daniel Bernoulli for sharing unpublished data of the Cellina section and for the discussion about the platform margin, and to A. Riva, for sharing some thoughts on the M. Cavallo clinoforms. A. Husinec is acknowledged for his positive comments on an earlier version of the manuscript. M. Cobianchi was financially supported by FAR 2015 – 2016 grants (Pavia University). V. Luciani was financially supported from Ferrara University (FAR 2016-2017 grants). The authors express their gratitude to the Journal reviewers, M. Morsilli and anonymous, for their thoughtful reviews.

References

Amodio, S., Weissert, H., 2017. Palaeoenvironment and palaeoecology before and at the onset of Oceanic Anoxic Event (OAE)1a: Reconstructions from Central Tethyan archives. Palaeogeogr. Palaeoclimatol. Palaeoecol. 479, 71-89.

Aubouin, J., 1970. Essai sur la géologie des Dinarides. Bull. Soc. Géol. Fr. 12, 1060-1095.

Bassani, F., 1886. Sull'età degli strati a pesci di Castellavazzo nel Bellunese. Bollettino della Società Geologica Italiana, 4: 143–148.

Bernasconi S.M., Müller I. A., Bergmann K.D., Breitenbach S. F. M., Fernandez, A., Hodell D. A., Jaggi M., Meckler A.N. Millan I., and Ziegler M., 2018. Reducing uncertainties in carbonate clumped isotope analysis through consistent carbonate-based standardization. Geochemistry Geophysics Geosystems 19, 2895-2914.

Bernoulli, D., Jenkyns, H.C., 1974. Alpine, Mediterranean and Central Atlantic Mesozoic facies in relation to the early evolution of the Tethys. In: Dott, R.H., Shaver, R.H., (Eds.), Modern and ancient geosynclinals Sedimentation, SEPM Sp. Pubbl. 19, 129-160.

Bersezio, R., Fornaciari, M., 1994. Syntectonic Upper Cretaceous deep-water sequences of the Lombardy Basin (Southern Alps, Northern Italy). Ecl. Geol. Helv. 87, 833–862.

Bertotti, G., Picotti, V., Bernoulli, D., Castellarin, A., 1993. From rifting to drifting: Tectonic evolution of the South-Alpine upper crust from the Triassic to the Early Cretaceous. Sed. Geol. 86, 53–76.

Bertotti, G., Picotti, V., Cloetingh, S., 1998. Lithospheric weakening during "retro-foreland" basin formation: tectonic evolution of the central South Alpine foredeep. Tectonics 17, 131-142.

Bornemann, A., Erbacher, J., Heldt, M., Wonik, T., 2017. The Albian-Cenomanian transition and Oceanic Anoxic Event 1d – an example from the Boreal Realm. Sedimentology 64(1), 44-65.

Bosellini, A., Morsilli, M., Neri, C., 1999. Long-term event stratigraphy of the Apulia Platform margin (Upper Jurassic to Eocene, Gargano, southern Italy). Journal of Sedimentary Research, 69 (6), pp. 1241-1252.

Bown, P.R., Young, J.R., 1998. Techniques. In: Bown, P.R. (Ed.), Calcareous nannofossil biostratigraphy, British Micropaleontological Society Publications Series, Kluwer Academic Publishers, London, 16-28.

Bralower, T.J., Leckie, R.M., Sliter, W.V., Thierstein, H.R., 1995. An integrated Cretaceous microfossil biostratigraphy – Geochronology Time Scales and Global Stratigraphic Correlation, SEPM Spec. Publ. 54, 65-79.

Brčić, V., Glumac, B., Fuček, L., Grizeli, A., Horvat, M., Posilović, H., Mišur, I., 2017. The Cenomanian–Turonian boundary in the northwestern part of the Adriatic Carbonate Platform (Ćićarija Mtn., Istria, Croatia): characteristics and implications. Facies 63, 17 -?.

Breitenbach, S., Bernasconi, S.M., 2011. Carbon and oxygen isotope analysis of small carbonate samples (20 to 100 μg) with a GasBench II preparation device – In: Rapid Commun. Mass Spectrom. 2011, 25, 1910– 1914

Burnett, J.A., 1998. Upper Cretaceous. In: Bown, P.R., (Ed.), Calcareous nannofossil biostratigraphy, British Micropaleontological Society Publications Series. Kluwer Academic Publishers, London, 132-199.

Carannante, G., Graziano, R., Ruberti, D., Simone, L., 1997. Upper Cretaceous temperate-type open shelves from northern (Sardinia) and southern (Apennines-Apulia) Mesozoic Tethyan margins. In: James, N.P., Clarke, J.A.D. (Eds.), Cool-water carbonates. SEPM Spec. Publ. 56, 309-325.

Cherchi, A., Schroder, R., 2013. The Praeorbitolina/Palorbitolinoides Association: an Aptian biostratigraphic key-interval at the southern margin of the Neo-Tethys. Cret. Res. 39, 70-77.

Chiocchini, M., Chiocchini R.A., Didaskalou, P., Potetti M., 2008. Microbiostratigrafia del Triassico superiore, Giurassico e Cretacico in facies di piattaforma carbonatica del Lazio centro-meridionale e Abruzzo: revisione finale. Mem. Descr. Carta Geol. It. 84, 5 – 170.

Cimolino, A., Della Vedova, B., Nicolich, R., Barison, E., Brancatelli, G., 2010. New evidence of the outer Dinaric deformation front in the Grado area (NE-Italy). Rend. Fis. Acc. Lincei, 21, 167 - 179.

Coccioni, R., Premoli Silva, I., 2015. Revised Upper Albian–Maastrichtian planktonic foraminiferal biostratigraphy and magneto- stratigraphy of the classical Tethyan Gubbio section (Italy). News. Strat. 48 (1), 47–90**.**

Costa, V., Doglioni, C., Grandesso, P., Masetti, D., Pellegrini, G.B., Tracanella, E., 1992. Note Illustrative del F˚063 Belluno. Servizio geologico d'Italia, 74 pp. http://www.isprambiente.gov.it/Media/carg/note_illustrative/63_Belluno.pdf

Costacurta, R., Grandesso, P., Massari, F., Medizza, F., 1979. Il Giurese Superiore-Cretaceo della regione compres tra Casso e Claut (Prealpi Carniche occidentali). Studi Trentini di Scienze Naturali, Geologia 56, 3-25.

Cuvillier, J., Foury, G., Pignatti Morano, A. 1968. Foraminifères nouveaux du Jurassique supérieur du Val Cellina (Frioul occidental, Italie). Geol. Romana 7, 141 - 156

Cvetko Tešović, B., Glumac, B., Bucković, D., 2011. Integrated biostratigraphy and carbon isotope stratigraphy of the Lower Cretaceous (Barremian to Albian) Adriatic-Dinaridic carbonate platform deposits in Istria, Croatia. Cretaceous Research 32, 301–324.

Davey S.D., Jenkyns H.C., 1999. Carbon-isotope stratigraphy of shallow-water limestones and implications for the timing of Late Cretaceous sea-level rise and anoxic events (Cenomanian–Turonian of the peri-Adriatic carbonate platform, Croatia). Ecl. Geol. Helv 92, 163–170.

de Leeuw, A., Mandic, O., Krijgsman, W., Kuiper, K., Hrvatovič, H., 2012. Paleomagnetic and geochronologic constraints on the geodynamic evolution of the Central Dinarides. Tectonophysics 530, 286–298.

Doglioni, C., 1992. The Venetian Alps thrust belt. In: McClay, K. R., (Ed), Thrust Tectonics, Chapman & Hall, London, 319-324.

Erba, E., 2004. Calcareous nannofossils and Mesozoic oceanic anoxic events. Mar. Micropaleontol. 52, 85-106.

Ferasin, F., 1958. Il « complesso di scogliera » cretaceo del Veneto centro-orientale. Mem. Istit. Geol. Mineral. Padova 21, 1-55.

Föllmi, K.B., Godet, A., Bodin, S., Linder, P., 2006. Interactions between environmental change and shallow-water carbonate build-up along the northern Tethyan margin and their impact on the early Cretaceous carbon-isotope record. Paleoceanography 21, 16 pp. doi:10.1029/2006PA001313

Föllmi, K.B., 2012. Early Cretaceous life, climate and anoxia. Cretaceous Research 35, 230-257.

Frijia, G, Parente, M. Di Lucia, M., Mutti, M., 2015. Carbon and strontium isotope stratigraphy of the Upper Cretaceous (Cenomanian-Campanian) shallow-water carbonates of southern Italy: Chronostratigraphic calibration of larger foraminifera biostratigraphy. Cretaceous Research, 53,110-139, ISSN 0195-6671, https://doi.org/10.1016/j.cretres.2014.11.002.

Gambacorta, G., Bersezio, R., Weissert, H., Erba, E., 2015. Onset and demise of Cretaceous oceanic anoxic events: the coupling of surface and bottom oceanic processes in two pelagic basins of the western Tethys. Paleoceanography 31, 732-757.

Ghetti, S., 1987. Evoluzione cretacica del margine occidentale della Piattaforma Friulana. PhD thesis, University of Ferrara, 205 pp.

Giorgioni, M., Weissert, H., Bernasconi, S.M., Hochuli, P.A., Keller, C.E., Coccioni, R., Petrizzo, M.R., Lukeneder, A., Garcia, T.T., 2015. Paleoceanographic changes during the Albian–Cenomanian in the Tethys and North Atlantic and the onset of the Cretaceous chalk. Glob. Planet. Change 126, 46–61.

Gnaccolini, M., 1968. Sedimentologia del Calcare di Soccher nella regione compresa tra la valle del T. Vajont (Pordenone) e l'Alpago (Belluno). Riv. It. Strat. Paleont. 74, 829-864.

Gušić, I., Jelaska V., 1993. Upper Cenomanian-Lower Turonian sea- level rise and its consequences on the Adriatic-Dinaric carbonate platform. Geol Rund. 82, 676–686.

Hallock, P., 2001. Coral Reefs, Carbonate Sediments, Nutrients, and Global Change. In: Stanley G.D. (Ed.), The History and Sedimentology of Ancient Reef Systems, Topics in Geobiology 17, Springer, Boston, 387 – 427.

Hönisch, B., Ridgwell, A., Schmidt, D.N., Thomas, H., Gibbs, S.J., Sluijs, A., Zeebe, R., Kump, L., Martindale, R.C., Greene, S.E., Kiessling, W., Ries, J., Zachos, J.C., Royer, L.D., Barker, S., Marchitto Jr., T.M., Moyer, R., Pelejero, C., Ziveri, P., Foster, G.L., Williams, B., 2012. The Geological record of Ocean Acidification. Science 335, 1058-1063.

Huck, S., Rameil, N., Korbar, T., Heimhofer, U., Wieczorek, T.D., Immenhauser, A., 2010. Latitudinally different responses of Tethyan shoal-water carbonate systems to the Early Aptian oceanic anoxic event (OAE 1a). Sedimentology 57, 1585–1614.

Hueter, A., Huck, S., Bodin, S., Heimhofer, U., Weyer, S., Jochum, K. P., and Immenhauser, A.: Central Tethyan platform-top hypoxia during Oceanic Anoxic Event 1a, Clim. Past Discuss., https://doi.org/10.5194/cp-2019-3, in review, 2019

Husinec, A., Read, J.F., 2018. Cyclostratigraphic and $\delta^{13}C$ record of the Lower Cretaceous Adriatic Platform, Croatia: a diagenetically overprinted Milankovitch-forced chemostratigraphic signal. Sedimentary Geology 373, 11-31.

Jarvis, I., Gale, A. S., Jenkyns, H. C., Pearce, M., 2006. Secular variations in Late Cretaceous carbon isotopes: a new $\delta^{13}C$ carbonate reference curve for the Cenomanian-Campanian (99.6–70.6 Ma). Geol. Mag.143, 561-608.

Jarvis, I., Lignum, J.S., Grocke, D.R., Jenkyns, H.C., 2011. Black shale deposition, atmospheric CO2 drawdown and cooling during the Cenomanian Oceanic Anoxic Event. Paleoceanography 26, PA3201.

Jenkyns, H.C., 1991. Impact of Cretaceous sea level rise and anoxic events on the Mesozoic carbonate platform of Yugoslavia. American Association of Petroleum Geologists Bulletin 75, 1007–1017.

Jenkyns, H.C., 2010. Geochemistry of Oceanic Anoxic Event. Geochem. Geophys. Geosyst. 11, Q03004. Doi:10.1029/2009GC002788.

Jenkyns, H.C., Dickson, A.J., Ruhl, M., Van Den Boorn, S.J.H.M. 2017. Basalt-seawater interaction, the Plenus Cold Event, enhanced weathering and geochemical change: deconstructing Oceanic Anoxic Event 2 (Cenomanian-Turonian, Late Cretaceous). Sedimentology 64, 16-43.

Jenkyns, H.C., 2018. Transient cooling episodes during Cretaceous Oceanic Anoxic Events with special reference to OAE 1a (Early Aptian). Philosophical Transactions of the Royal Society A 376, 20170073. http://dx.doi.org/10.1098/rsta.2017.0073

Kidder, D.L., Worsley, T.R., 2010. Phanerozoic Large Igneous Provinces (LIPs), HEATT (Haline Euxinic Acidic Thermal Transgression) episodes, and mass extinctions. Palaeogeogr. Palaeoclimatol. Palaeoecol. 295, 162-191.

Korbar, T., Glumac, B., Cvetko-Tešović, B., Cadieux, S.B., 2012. Response of a carbonate platform to the Cenomanian–Turonian drowning and OAE 2: a case study from the Adriatic Platform (Dalmatia, Croatia). J. Sediment. Res. 82, 163–176

Larson, R.L., Erba, E., 1999. Onset of the Mid-Cretaceous greenhouse in the Barremian-Aptian: Igneous events and the biological, sedimentary, and geochemical responses. Paleoceanography 14 (6), 663-678.

Luciani, V., Cobianchi, M., Jenkyns, H.C., 2004. Albian high-resolution biostratigraphy and isotope stratigraphy: The Coppa della Nuvola pelagic succession of the Gargano Promontory (Southern Italy). Ecl. Geol. Helv. 97, 77–92.

Luciani, V., Cobianchi, M., Lupi, C. 2006. Regional record of a global oceanic anoxic event: OAE1a on the Apulia Platform margin, Gargano Promontory, southern Italy. Cret. Res. 27, 754-772.

Lukeneder, A., 2010. Lithostratigraphic definition and stratotype for the Puez Formation: formalisation of the Lower Cretaceous in the Dolomites (S. Tyrol, Italy). Austrian J. Earth Sci., 103/1, 138-158.

Masetti, D., Fantoni, R., Romano, R., Sartorio, D., & Trevisani, E. (2012). Tectonostratigraphic evolution of the Jurassic extensional basins of the eastern southern Alps and Adriatic foreland based on an integrated study of surface and subsurface data. AAPG Bull., 96, 2065–2089.

Menegatti, A.P., Weissert, H., Brown, R.S., Tyson, R.V., Farrimond, P., Strasser, A., Caron, M., 1998. High- resolution $\delta^{13}C$ stratigraphy through the early Aptian “Livello Selli” of the Alpine Tethys. Paleoceanography 13 (5), 530–545.

Mellere, D., Stefani, C., Angevine, C., 2000. Polyphase tectonics through subsidence analysis: the Oligo-Miocene Venetian and Friuli Basin, north-east Italy. Basin Res. 12, 159–182.

Millán, M.I., Weissert, H.J., López-Horgue, M.A., 2009. Expression of the late Aptian cold snaps and the OAE1b in a highly subsiding carbonate platform (Aralar, northern Spain). Palaeogeogr. Palaeoclimatol. Palaeoecol. 411, 167–179.

Millán, M.I., Weissert, H.J., Fernández-Mendiola, P.A., García-Mondéjar, J., 2014. Impact of Early Aptian carbon cycle perturbations on evolution of a marine shelf system in the Basque-Cantabrian Basin (Aralar, N Spain). Earth and Planet. Sci. Lett. 287, 392-401.

Mutti, M., Hallock, P., 2003. Carbonate systems along nutrient and temperature gradients: some sedimentological and geochemical constraints. Int. J. Earth Sci. 92, 465–475.

Otoničar, B., 2007. Upper Cretaceous to Paleogene Forbulge Unconformity associated with Foreland Basin evolution (Kras, Matarsko Podolje and Istria; SW Slovenia and NW Croatia). Time in Karst, Postojna, 101–120.

Ogg, J.G., Hinnov, L.A., 2012. Cretaceous. The Geological Time Scale 2012. In: Gradstein, F.M., Ogg, J.G., Schmitz, M.D., Ogg, G.M. (Eds.), 2012. Elsevier, Amsterdam, 793-853.

Pamić, J., Gušić, I., Jelaska, V., 1998. Geodynamic evolution of the Central Dinarides. Tectonophysics 297, 251– 268.

Parente M, Frijia G., Di Lucia M., Jenkyns H. C., Richard G. Woodfine R. G, Barboncini F., 2008. Stepwise extinction of larger foraminifera at the Cenomanian–Turonian boundary: a shallow water perspective on nutrient fluctuations during Oceanic Anoxic Event 2 (Bonarelli Event). Geology, v. 36 (9), 715-718.

Phelps, R.M., Kerans, C., Da-Gama, R.O.B.P., Jeremiah, J., Hull, D., Loucks, R.G., 2015. Response and recovery of the Comanche carbonate platform surrounding multiple Cretaceous oceanic anoxic events, northern Gulf of Mexico. Cret. Res. 54, 117-144.

Picotti, V., Cobianchi, M., 2017. Jurassic stratigraphy of the Belluno Basin and Friuli Platform: a perspective on far-field compression in the Adria passive margin. Swiss J. Geosci. 110, 833-850.

Pomar, L., 2001. Types of carbonate platforms: a genetic approach. Basin Res. 13, 313-334.

Rameil, N., Immenhauser, A., Warrlich, G., Hillgärtner, H., Droste, H.J., 2010. Morphological patterns of Aptian *Lithocodium-Bacinella* geobodies: Relation to environment and scale. Sedimentology, 57(3),883-911.

Riva, M., Besio, M., Masetti, D., Roccati, F., Sapigni, M., Semenza, E., 1990. La geologia delle valli del Vajont e Gallina. Annali Univ. Ferrara, Sc. della Terra 2, 4, 55-76.

Roth, P.H., 1978. Cretaceous nannoplankton biostratigraphy and oceanography of the northwestern Atlantic Ocean. In: Benson, W.E., Sheridan, R.E., et al., (Eds.), Init. Repts. DSDP 44, Washington (U.S. Govt. Printing Office), 731–759.

Schindler, U., Conrad, M., 1994. The Lower Cretaceous Dasycladales from the Northwestern Friuli Platform and their Distribution in Chronostratigraphic and Cylcostratigraphic Units. Rev. Paléobiol. 13, 59-96.

Schlager, W. Benthic carbonate factories of the Phanerozoic. Int. J. Earth Sci. (Geol Rundsch) (2003) 92: 445. https://doi.org/10.1007/s00531-003-0327-x

Schlanger, S.O., Jenkyns, H.C., 1976. Cretaceous Oceanic Anoxic Events: causes and consequences. Geol. Mijnbouw 55, 179–184.

Schlanger, S.O., Arthur, M.A., Jenkyns, H.C., Scholle, P.A., 1987. The Cenomanian-Turonian Oceanic Anoxic Event, I. In: Brooks, J., Fleet, A.J. (Eds.), Stratigraphy and distribution of organic carbon-rich beds and the marine ∂^{13}C excursion, Marine Petroleum Source Rocks, Geol. Soc. Spec. Publ. 26, 371-399.

Scholle, P.A., Arthur, M.A., 1980. Carbon isotope fluctuations in Cretaceous pelagic limestones: potential stratigraphic and petroleum exploration tool. AAPG Bull. 64, 67–87.

Skelton, P.W., Gili, E., 2012. Rudists and carbonate platforms in the Aptian: a case study on biotic interactions with ocean chemistry and climate. Sedimentology 59, 81-117.

Sissingh, W., 1977. Biostratigraphy of Cretaceous calcareous nannoplankton. Geol. Mijnbouw 51, 37-65.

Sprovieri, M., Sabatino, N., Pelosi, N., Batemburg, S.J., Coccioni, R., Iavarone, M., Mazzola, S. 2013. Late Cretaceous orbitally-paced carbon isotope stratigraphy from the Bottaccione Gorge (Italy). Palaeogeogr. Palaeoclimatol. Palaeoecol. 379, 81-94.

Stoll, H. M., Schrag, D. P., 2000. High-resolution stable isotope records from the Upper Cretaceous rocks of Italy and Spain: Glacial episodes in a greenhouse planet? Geol. Soc. Am. Bull.112, 309–319.

Thibault, N., Jarvis, I., Voigt, S., Gale, A. S., Attree, K., Jenkyns, H.C., 2016. Astronomical calibration and global correlation of the Santonian (Cretaceous) based on the marine carbon-isotope record. Paleoceanography 31, 847-865.

Tišljar, J., Vlahović, I., Velić, I., Matičec, D., Robson, J., 1998. Carbonate facies evolution from the Late Albian to Middle Cenomanian in southern Istria (Croatia): influence of synsedimentary tectonics and extensive organic carbonate production. Facies 38, 137-152.

Vlahović, I., Tišljar, J., Velić, I., Matičec, D., 2005. Evolution of the Adriatic Carbonate Platform: Palaeogeography, main events and depositional dynamics. Palaeogeogr. Palaeoclimatol. Palaeoecol. 220, 333-360.

ViDEPI, http://www.videpi.com/videpi/videpi.asp

Voigt, S., Friedrich, O., Norris, R.D., Schönfeld, J., 2010. Campanian–Maastrichtian carbon isotope stratigraphy: shelf-ocean correlation between the European shelf sea and the tropical Pacific Ocean. Newslet. Stratigr. 44, 57–72.

Weissert, H., 1989. C-isotope stratigraphy, a monitor of paleoenvironmental change: a case study from the Early Cretaceous. Survey Geophysics 10, 1-61.

Weissert, H., Erba, E., 2004. Volcanism, CO_2 and paleoclimate: a Late Jurassic-Early Cretaceous carbon and oxygen isotope record. J. Geol. Soc. London 161, 695-702.

Weissert, H., Lini, A., Föllmi, K.B., Kuhn, O., 1998. Correlation of Early Cretaceous carbon isotope stratigraphy and platform drowning events: a possible link? Palaeogeogr. Palaeoclimatol. Palaeoecol. 137, 189-203.

Wisler, L., Funk, H., Weissert, H., 2003. Response of Early Cretaceous carbonate platforms to changes in atmospheric carbon dioxide levels. Palaeogeogr. Palaeoclimatol. Palaeoecol. 200, 187-205.

Woodfine, R.G. 2002. Chemostratigraphy of Jurassic-Cretaceous Italian Carbonate Platform. PhD thesis. University of Oxford, 383 pp.

Zanchetta, S., Malusà, M.G., Zanchi, A., 2015. Precollisional development and Cenozoic evolution of the Southalpine retrobelt (European Alps). Lithosphere, 662-681.

FIGURE CAPTIONS

Fig. 1 – Cretaceous paleogeographic domains projected over the present-day topography (not retrodeformed) and location of the Puez, Casso and Cellina sections (Fig. 4 and 5; Fig. 7). The red, dashed line represents the post-Albian coastal onlap, reconstructed on the base of Cenomanian - Maastrichtian stratigraphic gaps found in wells to the north (Nervesa, Grado), and outcrops in Istria (Brčić et al., 2017), whereas continuous succession are found at Cargnacco (small full circles).

Fig. 2 - A stratigraphic chart of the northwestern margin of the Friuli-Adriatic Carbonate Platform, integrated with our observations and modified after Schindler and Conrad (1994), who dated the units mainly by means of dasycladacean algae. Note the important backstep of the margin at the Cenomanian. The names refer to the localities described by the above quoted authors. Note the horizontal and the vertical scales are the same.

Fig. 3 – Summary of different stage boundaries with numerical ages and calcareous nannofossil and planktic foraminifer biostratigraphic zonations for the Aptian-Campanian interval. The position of the GSSPs according to the various authors is reported.

Fig. 4 – Litho-, bio-, and carbonate carbon isotope stratigraphy from the Casso section. Biostratigraphy is based on planktic foraminifera (bioevents in bold) and calcareous nannofossils (bioevents in regular). For the carbon isotope record, black line connected the data points of all samples analysed; thin blue line represents a two-point moving average; thick red and blue lines are for long-term trends. Key isotope events are marked by purple and green shading.

Fig. 5 - Litho- and biostratigraphy of the Val Cellina section. Bold: new data. The names close to the biostratigraphic data refer to the two authors: Bruni in Woodfine, 2002; Ghetti, 1987. C-S is for Coniacian – Santonian; C-M is for Campanian – Maastrichtian.

Fig. 6 - Field aspects of the Cenomanian mounds in the Val Cellina section. a) Mound at around 1190 m, looking southwest. Note the clinoform at the northern margin and the occurrence of another mound body at slightly lower stratigraphic level in the far background. b) Mound at around 1235 at the confluence of the Molassa creek intro the Cellina river, looking south. Note the clinoforms at the base and the onlap of the intramound clastics from the west. c) Detail of the thin section CE19 Y, showing the *Bacinella/Lithocodium* encrusting microproblematica.

Fig. 7 – Subsidence history of the platform margin at Val Cellina compared to the composite section Istria, taken from Vlahovič et al. (2005), and the measured section Puez, after Lukeneder (2010). See Fig. 1 for the location of the measured/composite sections. The points of the section Val Cellina are associated to error bars, due to the uncertainties in the chronostratigraphic calibrations.

Fig. 8 (A and B) – Carbon-isotope stratigraphy for the Barremian - Albian (A) and Albian - Cenomanian (B) from the Casso section (this study; black line: all data points, grey line: two point moving average) compared to the $\delta^{13}C$ curves for the Cismon and Piobbico sections (Weissert et al, 1998) and to the stacked composite curve for the English Chalk section (Jarvis et al., 2006). NC zones are for calcareous nannofossil zonation (Bralower et al., 1995). The position of the OAE1a (green shading) and OAE 1d (purple shading) in the the Casso isotope record is shown.

Fig. 9 – Carbon-isotope stratigraphy for the Albian – Turonian from the Casso section (this study; black line: all data points, grey line: two point moving average) compared to the $\delta^{13}C$ stacked composite curve for the English Chalk section (Jarvis et al., 2006) and for the Contessa Quarry section (Stoll and Schrag, 2000). NC zones are for calcareous nannofossil zonation (Bralower et al., 1995). Note the OAE2 (purple shading) and the possible Caburn, Bridgewick, HitchWood and Navigations Events (light and dark green shading) in the Casso isotopic curve.

Fig. 10 – Carbon-isotope stratigraphy for the Coniacian – Santonian from the Casso section (this study; all data points) compared to the $\delta^{13}C$ stacked composite curve for the English Chalk section (Jarvis et al., 2006) and for the Bottaccione section (black line is for Thibault et al., 2016, all data points, pink line is for Sprovieri et al., 2013, 10 point moving average). Blue and red thick lines represent general trends in the isotope ratios. NC zones are for calcareous nannofossil zonation (Bralower et al., 1995).

Fig. 11 – a) Geometry of the rimmed margin of the Friuli-Adriatic Carbonate Platform at the end of the Albian. Note that normal faults, although widespread, likely did not control the location of the platform margin. b) Geometry of the distally steepened ramp at the end of the Cenomanian. The platform was tilted toward the NW, and was emerged to the SW. New faults were active toward the Belluno Basin, with the formation of local structural highs (Castellavazzo). Vertical exaggeration 10x.

Supplementary materials

1 calcareous nannofossil range chart

2 list of fossil species

3 chronostratigraphy of the Casso section

4 carbon isotope data

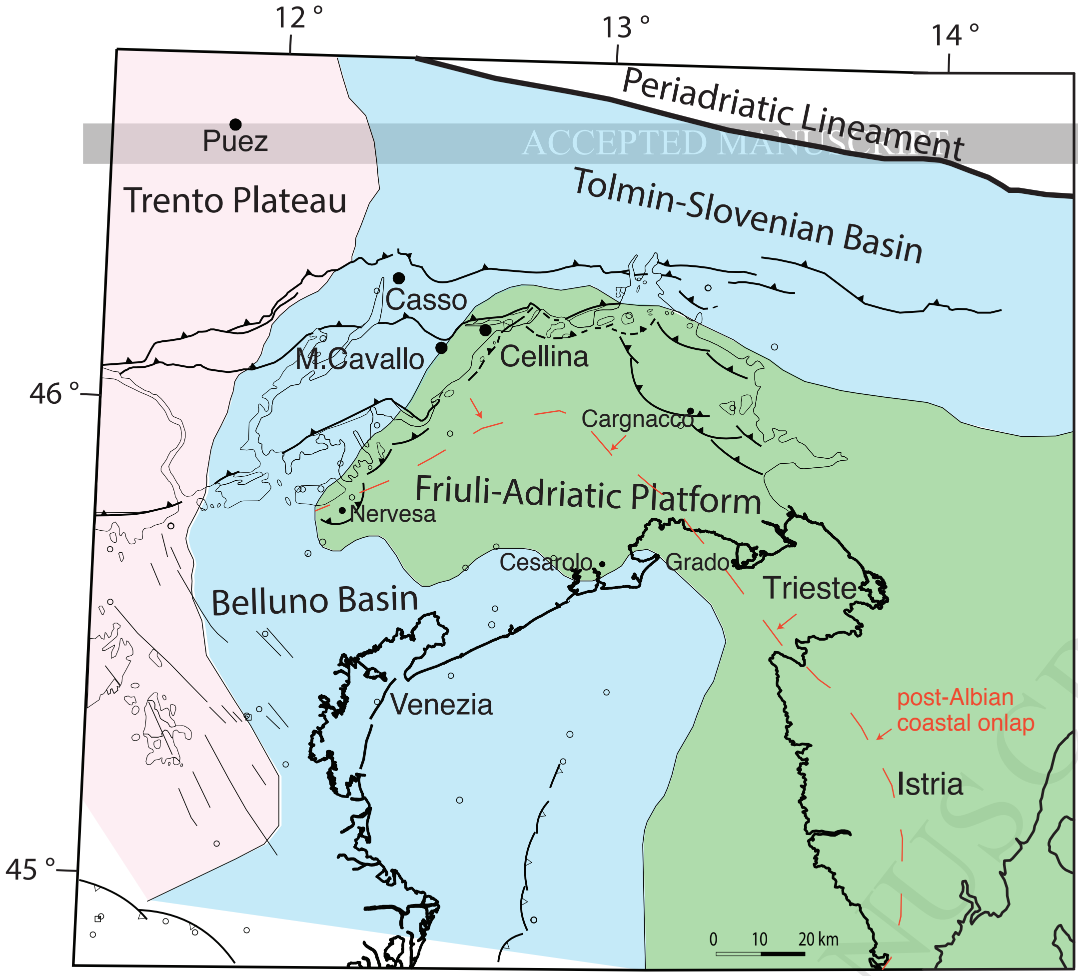
12 °
13 °
14 °
46 °
45 °
Periadriatic Lineament
Puez
Trento Plateau
Tolmin-Slovenian Basin
Casso
M.Cavallo
Cellina
Cargnacco
Friuli-Adriatic Platform
Nervesa
Cesarolo
Grado
Trieste
Belluno Basin
Venezia
post-Albian
coastal onlap
Istria
0 10 20 km

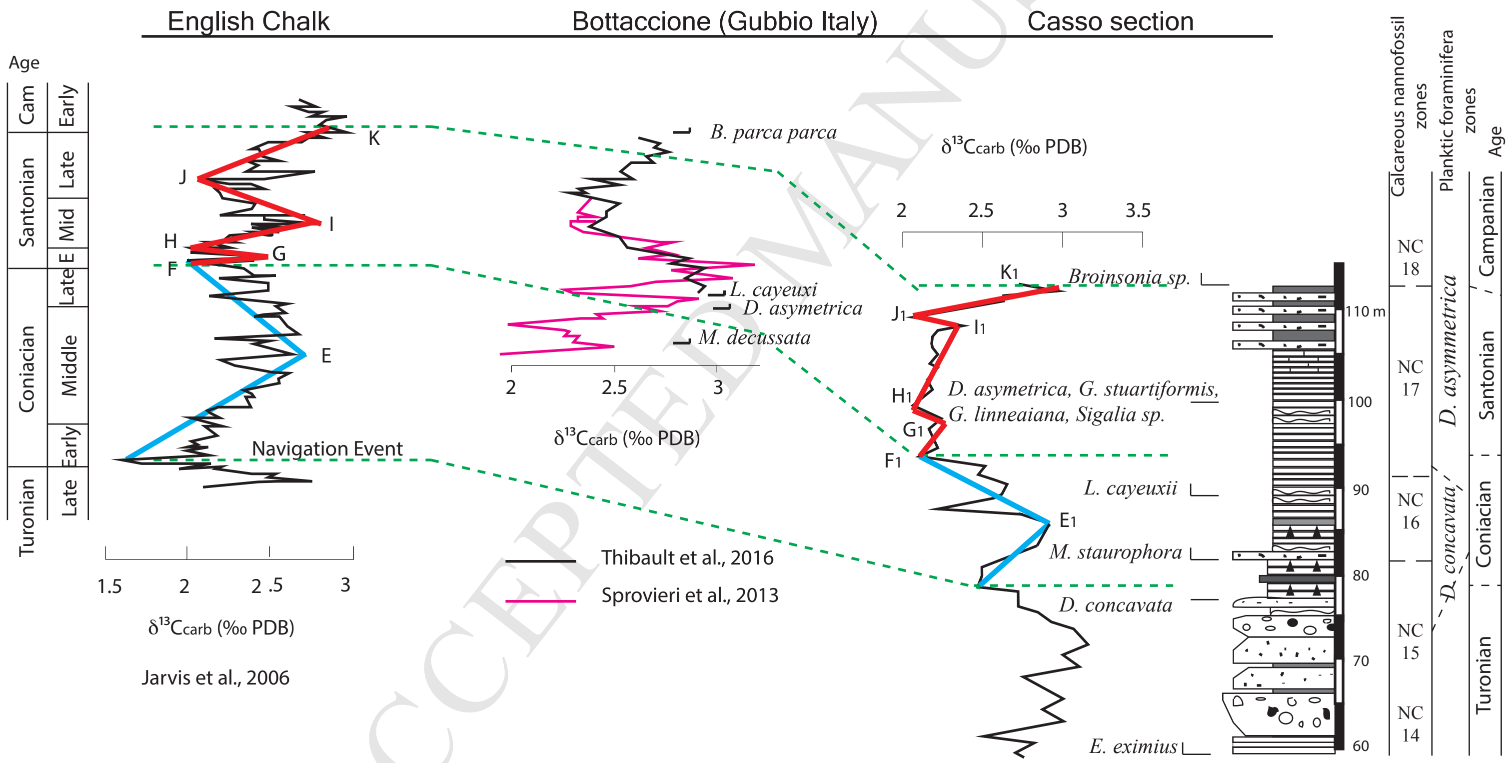
English Chalk
Bottaccione (Gubbio Italy)
Casso section
Age
Cam
Early
Santonian
Late
Mid
E
Coniacian
Late
Middle
Early
Turonian
Late
K
J
I
H
G
F
E
Navigation Event
1.5
2
2.5
3
δ13Ccarb (‰ PDB)
Jarvis et al., 2006
B. parca parca
L. cayeuxi
D. asymetrica
M. decussata
2
2.5
3
δ13Ccarb (‰ PDB)
Thibault et al., 2016
Sprovieri et al., 2013
δ13Ccarb (‰ PDB)
2
2.5
3
3.5
K1
Broinsonia sp.
J1
I1
D. asymetrica, G. stuartiformis,
G. linneaiana, Sigalia sp.
H1
G1
F1
L. cayeuxii
E1
M. staurophora
D. concavata
E. eximius
110 m
100
90
80
70
60
Calcareous nannofossil zones
NC 18
NC 17
NC 16
NC 15
NC 14
Planktic foraminifera zones
D. asymmetrica
D. concavata
Age
Campanian
Santonian
Coniacian
Turonian

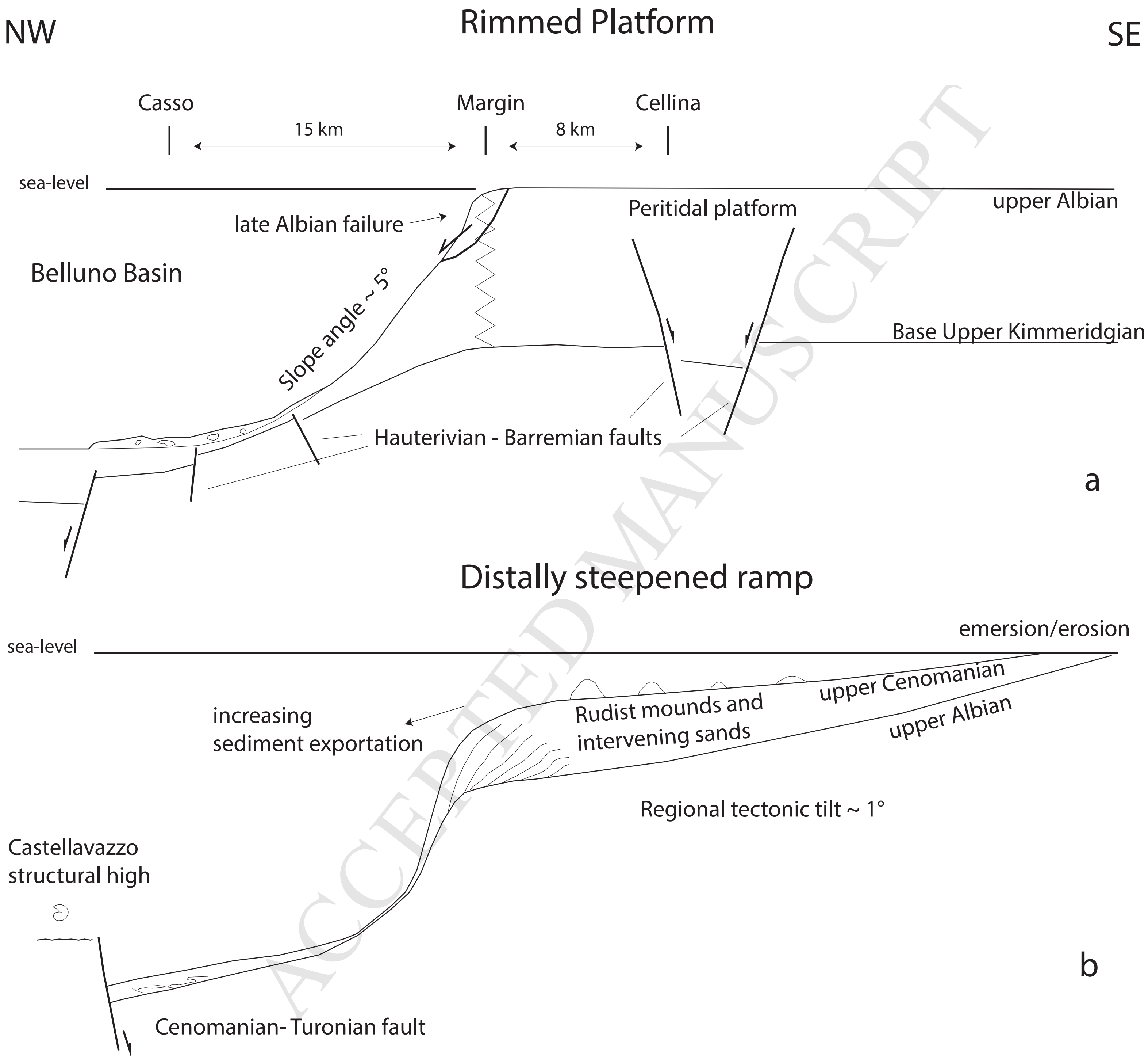
NW
Rimmed Platform
SE
Casso
Margin
Cellina
15 km
8 km
sea-level
upper Albian
late Albian failure
Peritidal platform
Belluno Basin
Slope angle ~ 5°
Base Upper Kimmeridgian
Hauterivian - Barremian faults
a
Distally steepened ramp
sea-level
emersion/erosion
upper Cenomanian
increasing
sediment exportation
Rudist mounds and
intervening sands
upper Albian
Regional tectonic tilt ~ 1°
Castellavazzo
structural high
b
Cenomanian- Turonian fault

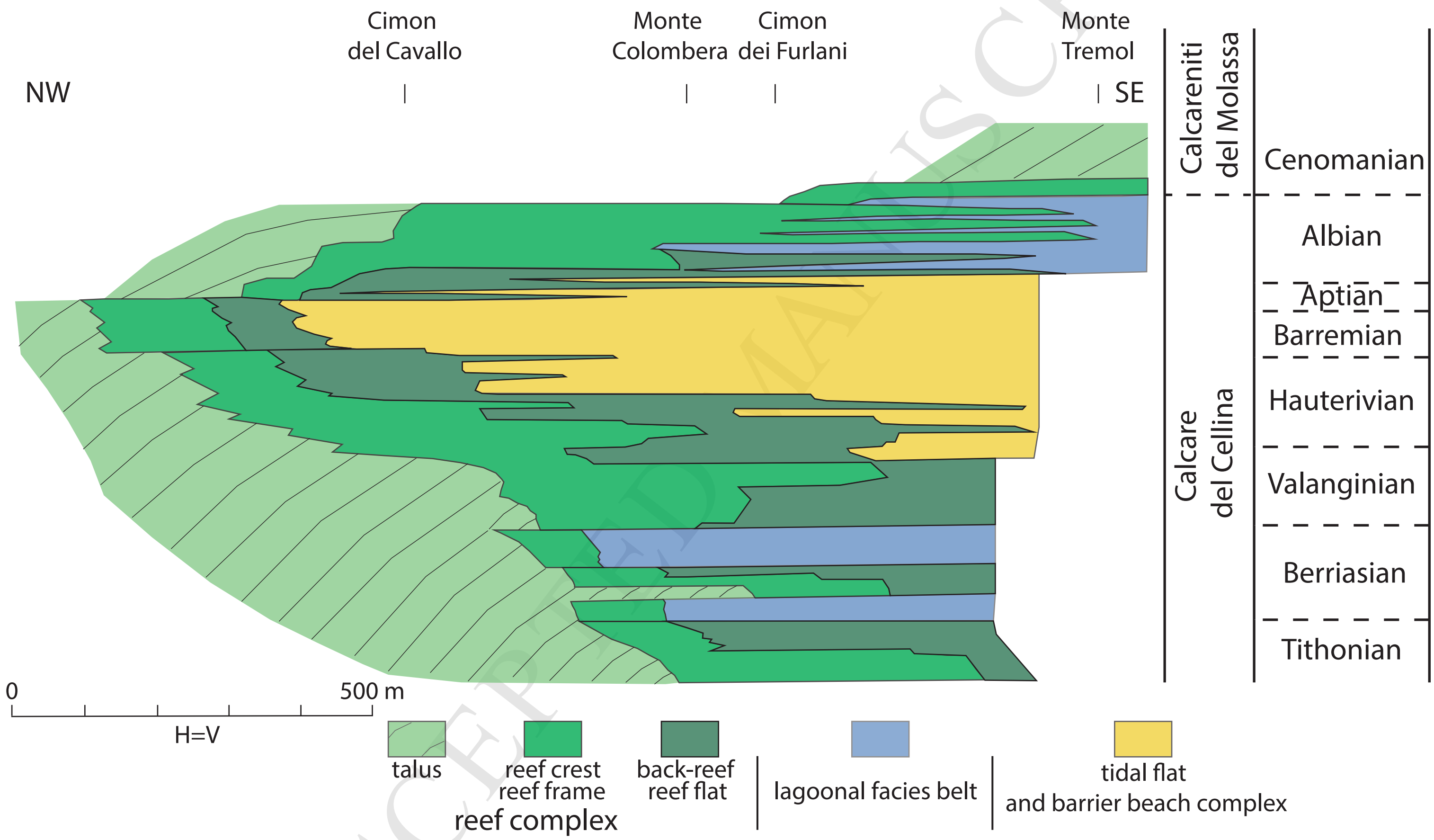

Cimon
del Cavallo
Monte
Colombera
Cimon
dei Furlani
Monte
Tremol
NW
SE
Calcareniti
del Molassa
Calcare
del Cellina
Cenomanian
Albian
Aptian
Barremian
Hauterivian
Valanginian
Berriasian
Tithonian
0
500 m
H=V
talus
reef crest
reef frame
back-reef
reef flat
reef complex
lagoonal facies belt
tidal flat
and barrier beach complex

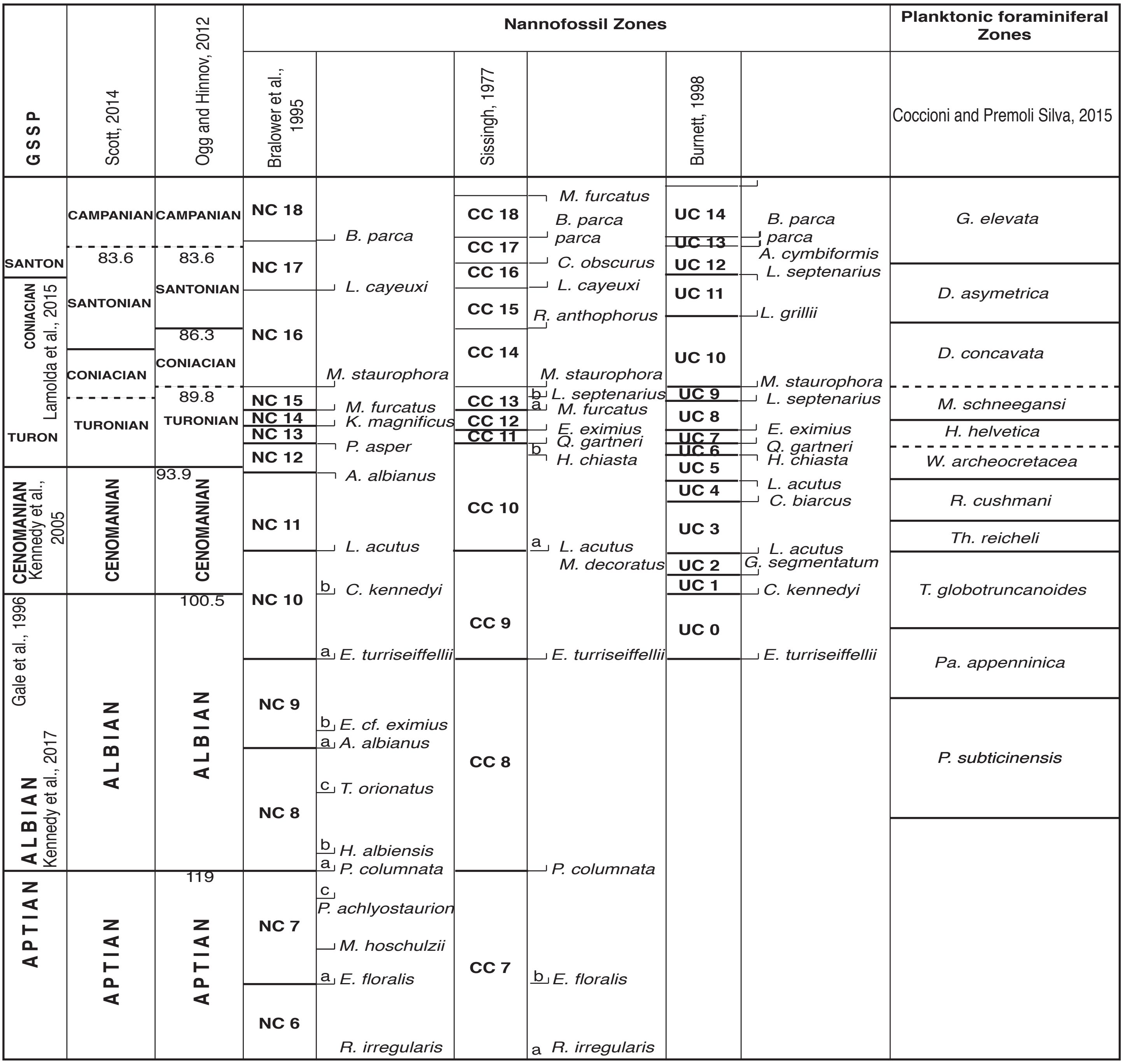

Nannofossil Zones
Planktonic foraminiferal Zones
G S S P
Scott, 2014
Ogg and Hinnov, 2012
Bralower et al., 1995
Sissingh, 1977
Burnett, 1998
Coccioni and Premoli Silva, 2015
SANTON
CONIACIAN
Lamolda et al., 2015
TURON
CENOMANIAN
Kennedy et al., 2005
Gale et al., 1996
ALBIAN
Kennedy et al., 2017
APTIAN
CAMPANIAN
SANTONIAN
CONIACIAN
TURONIAN
CENOMANIAN
ALBIAN
APTIAN
83.6
86.3
89.8
93.9
100.5
119
NC 18
NC 17
NC 16
NC 15
NC 14
NC 13
NC 12
NC 11
NC 10
NC 9
NC 8
NC 7
NC 6
B. parca
L. cayeuxi
M. staurophora
M. furcatus
K. magnificus
P. asper
A. albianus
L. acutus
b C. kennedyi
a E. turriseiffellii
b E. cf. eximius
a A. albianus
c T. orionatus
b H. albiensis
a P. columnata
c P. achlyostaurion
M. hoschulzii
a E. floralis
R. irregularis
CC 18
CC 17
CC 16
CC 15
CC 14
CC 13
CC 12
CC 11
CC 10
CC 9
CC 8
CC 7
M. furcatus
B. parca parca
C. obscurus
L. cayeuxi
R. anthophorus
M. staurophora
b L. septenarius
a M. furcatus
E. eximius
Q. gartneri
b H. chiasta
a L. acutus
M. decoratus
E. turriseiffellii
P. columnata
b E. floralis
a R. irregularis
UC 14
UC 13
UC 12
UC 11
UC 10
UC 9
UC 8
UC 7
UC 6
UC 5
UC 4
UC 3
UC 2
UC 1
UC 0
B. parca parca
A. cymbiformis
L. septenarius
L. grillii
M. staurophora
L. septenarius
E. eximius
Q. gartneri
H. chiasta
L. acutus
C. biarcus
L. acutus
G. segmentatum
C. kennedyi
E. turriseiffellii
G. elevata
D. asymetrica
D. concavata
M. schneegansi
H. helvetica
W. archeocretacea
R. cushmani
Th. reicheli
T. globotruncanoides
Pa. appenninica
P. subticinensis

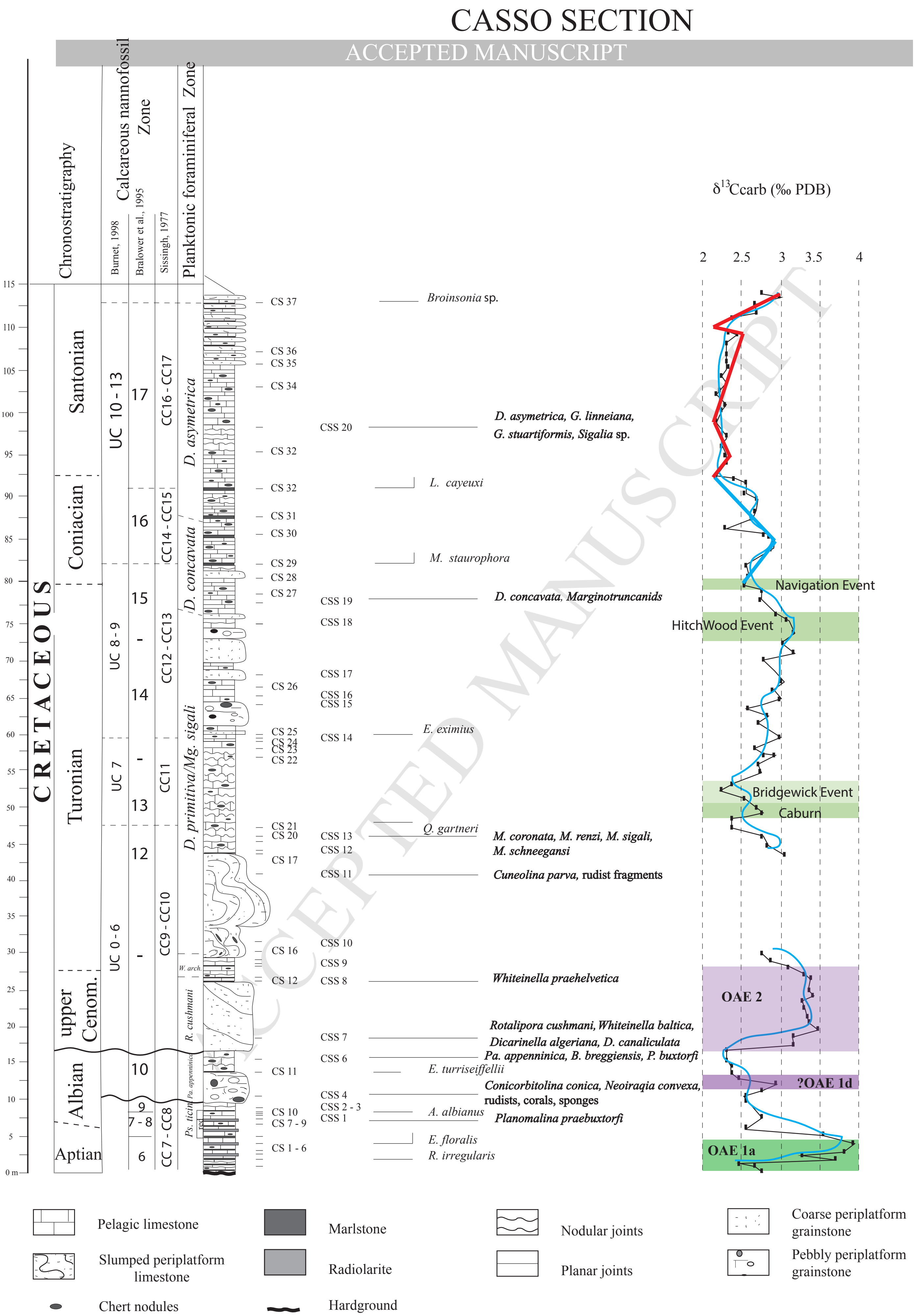
CASSO SECTION
Chronostratigraphy
Calcareous nannofossil Zone
Burnet, 1998
Bralower et al., 1995
Sissingh, 1977
Planktonic foraminiferal Zone
δ13Ccarb (‰ PDB)
2
2.5
3
3.5
4
CRETACEOUS
Santonian
Coniacian
Turonian
upper Cenom.
Albian
Aptian
UC 10 - 13
UC 8 - 9
UC 7
UC 0 - 6
17
16
15
14
13
12
10
9
7 - 8
6
CC16 - CC17
CC14 - CC15
CC12 - CC13
CC11
CC9 - CC10
CC 7 - CC8
D. asymetrica
D. concavata
D. primitiva/Mg. sigali
W. arch.
R. cushmani
Pa. appenninica
Ps. ticini
CS 37
CS 36
CS 35
CS 34
CS 32
CS 31
CS 30
CS 29
CS 28
CS 27
CS 26
CS 25
CS 24
CS 23
CS 22
CS 21
CS 20
CS 17
CS 16
CS 12
CS 11
CS 10
CS 7 - 9
CS 1 - 6
CSS 20
CSS 19
CSS 18
CSS 17
CSS 16
CSS 15
CSS 14
CSS 13
CSS 12
CSS 11
CSS 10
CSS 9
CSS 8
CSS 7
CSS 6
CSS 4
CSS 2 - 3
CSS 1
Broinsonia sp.
D. asymetrica, G. linneiana,
G. stuartiformis, Sigalia sp.
L. cayeuxi
M. staurophora
D. concavata, Marginotruncanids
E. eximius
Q. gartneri
M. coronata, M. renzi, M. sigali,
M. schneegansi
Cuneolina parva, rudist fragments
Whiteinella praehelvetica
Rotalipora cushmani, Whiteinella baltica,
Dicarinella algeriana, D. canaliculata
Pa. appenninica, B. breggiensis, P. buxtorfi
E. turriseiffellii
Conicorbitolina conica, Neoiraqia convexa,
rudists, corals, sponges
A. albianus
Planomalina praebuxtorfi
E. floralis
R. irregularis
Navigation Event
HitchWood Event
Bridgewick Event
Caburn
OAE 2
?OAE 1d
OAE 1a
115
110
105
100
95
90
85
80
75
70
65
60
55
50
45
40
35
30
25
20
15
10
5
0 m
Pelagic limestone
Slumped periplatform limestone
Chert nodules
Marlstone
Radiolarite
Hardground
Nodular joints
Planar joints
Coarse periplatform grainstone
Pebbly periplatform grainstone

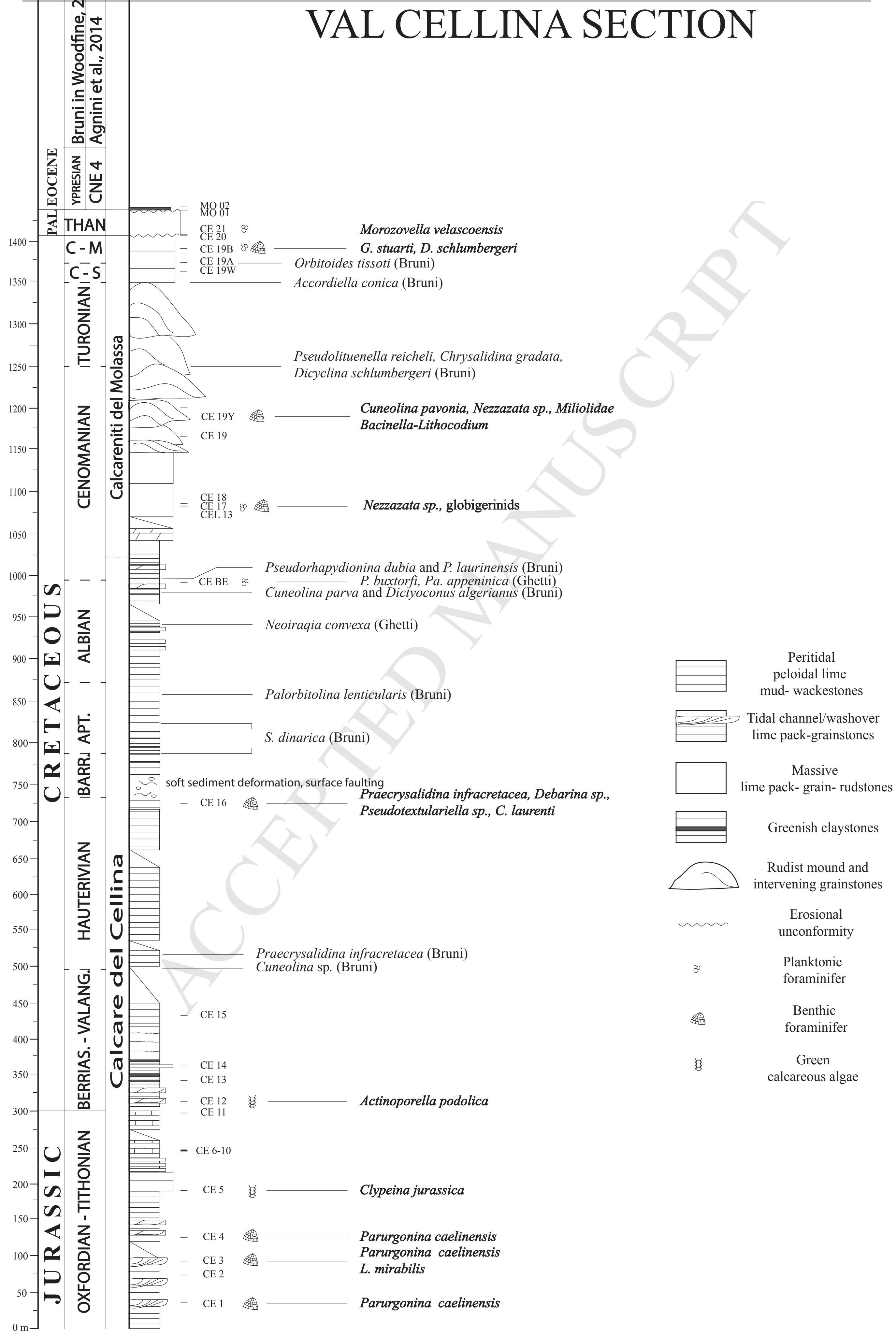

VAL CELLINA SECTION
Bruni in Woodfine, 2002
Agnini et al., 2014
EOCENE
YPRESIAN
CNE 4
PAL
THAN
C - M
C - S
TURONIAN
CENOMANIAN
ALBIAN
APT.
BARR.
HAUTERIVIAN
BERRIAS. - VALANG.
OXFORDIAN - TITHONIAN
CRETACEOUS
JURASSIC
Calcareniti del Molassa
Calcare del Cellina
1400
1350
1300
1250
1200
1150
1100
1050
1000
950
900
850
800
750
700
650
600
550
500
450
400
350
300
250
200
150
100
50
0 m
MO 02
MO 01
CE 21
CE 20
CE 19B
CE 19A
CE 19W
CE 19Y
CE 19
CE 18
CE 17
CEL 13
CE BE
CE 16
CE 15
CE 14
CE 13
CE 12
CE 11
CE 6-10
CE 5
CE 4
CE 3
CE 2
CE 1
Morozovella velascoensis
G. stuarti, D. schlumbergeri
Orbitoides tissoti (Bruni)
Accordiella conica (Bruni)
Pseudolituenella reicheli, Chrysalidina gradata,
Dicyclina schlumbergeri (Bruni)
Cuneolina pavonia, Nezzazata sp., Miliolidae
Bacinella-Lithocodium
Nezzazata sp., globigerinids
Pseudorhapydionina dubia and P. laurinensis (Bruni)
P. buxtorfi, Pa. appeninica (Ghetti)
Cuneolina parva and Dictyoconus algerianus (Bruni)
Neoiraqia convexa (Ghetti)
Palorbitolina lenticularis (Bruni)
S. dinarica (Bruni)
soft sediment deformation, surface faulting
Praecrysalidina infracretacea, Debarina sp.,
Pseudotextulariella sp., C. laurenti
Praecrysalidina infracretacea (Bruni)
Cuneolina sp. (Bruni)
Actinoporella podolica
Clypeina jurassica
Parurgonina caelinensis
Parurgonina caelinensis
L. mirabilis
Parurgonina caelinensis
Peritidal peloidal lime mud- wackestones
Tidal channel/washover lime pack-grainstones
Massive lime pack- grain- rudstones
Greenish claystones
Rudist mound and intervening grainstones
Erosional unconformity
Planktonic foraminifer
Benthic foraminifer
Green calcareous algae

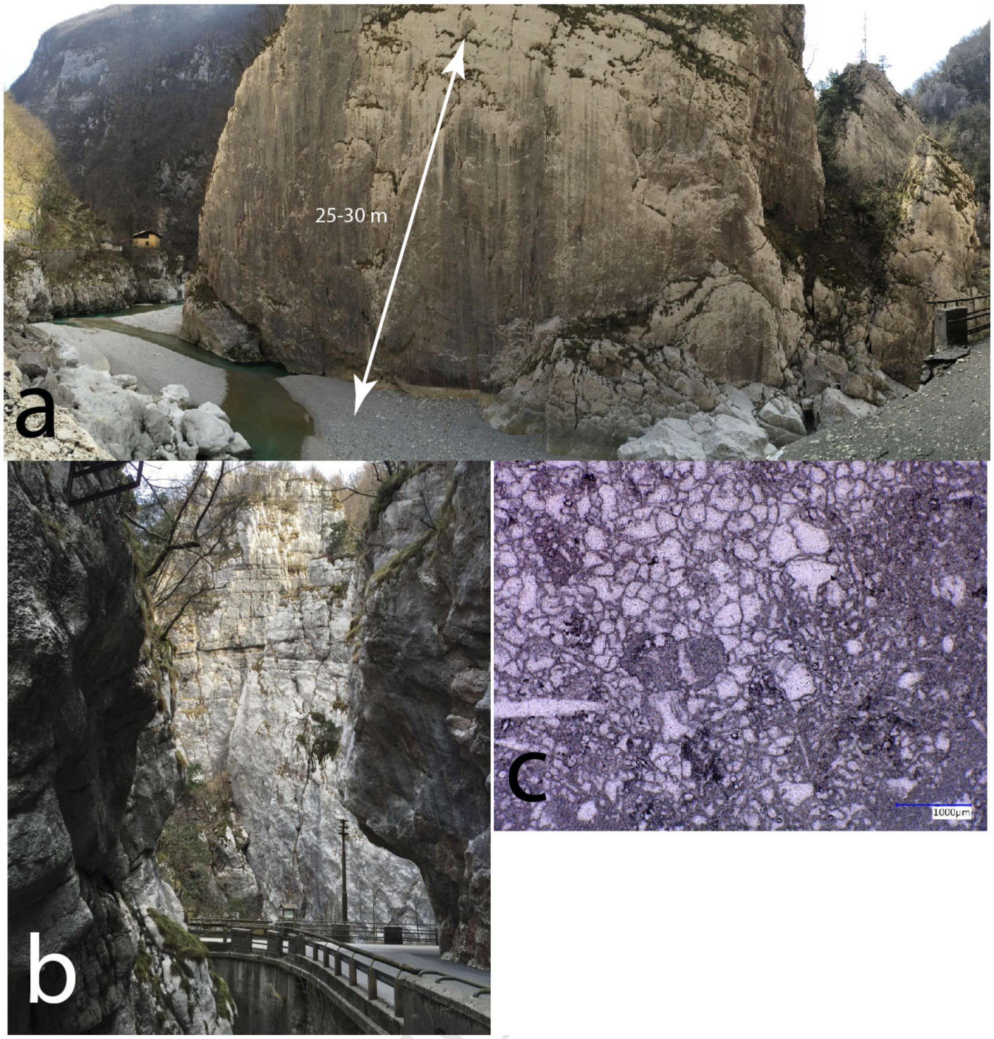
25-30 m
a
b
c
1000µm

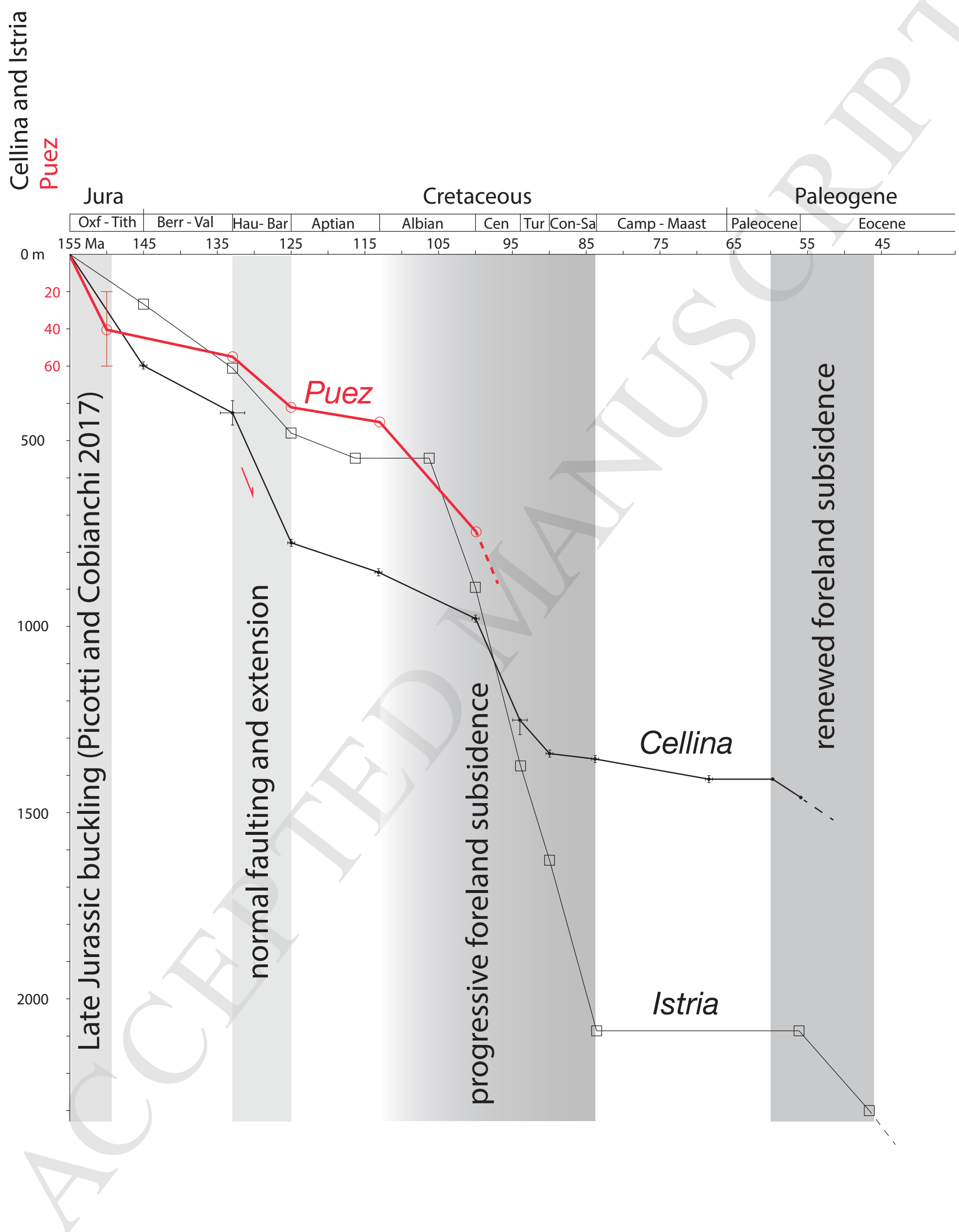

Cellina and Istria
Puez
Jura
Cretaceous
Paleogene
Oxf - Tith
Berr - Val
Hau- Bar
Aptian
Albian
Cen
Tur
Con-Sa
Camp - Maast
Paleocene
Eocene
155 Ma
145
135
125
115
105
95
85
75
65
55
45
0 m
20
40
60
500
1000
1500
2000
Puez
Cellina
Istria
Late Jurassic buckling (Picotti and Cobianchi 2017)
normal faulting and extension
progressive foreland subsidence
renewed foreland subsidence

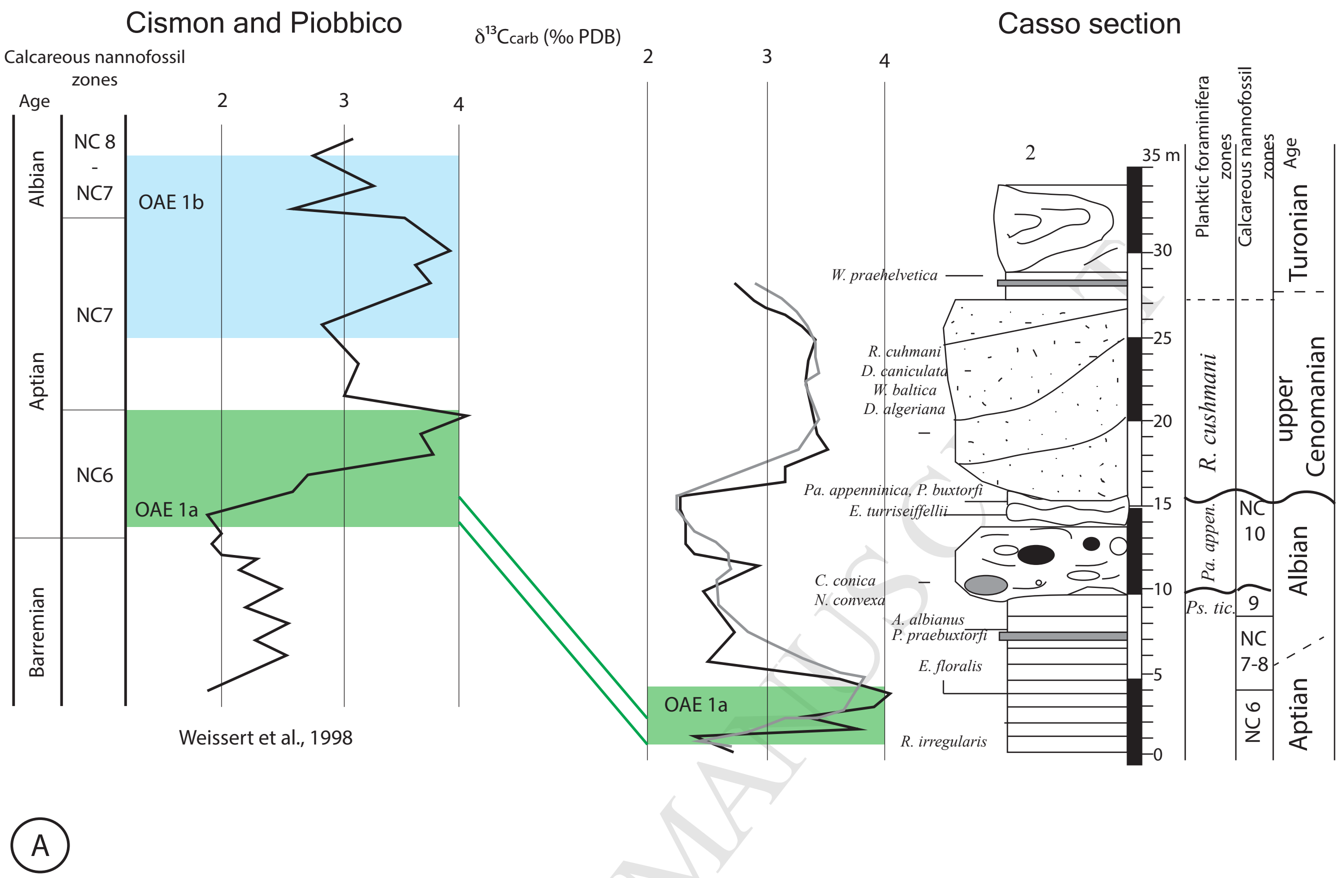

Cismon and Piobbico
Calcareous nannofossil zones
Age
δ13Ccarb (‰ PDB)
2
3
4
Albian
Aptian
Barremian
NC 8 - NC7
NC7
NC6
OAE 1b
OAE 1a
Weissert et al., 1998
Casso section
35 m
30
25
20
15
10
5
0
W. praehelvetica
R. cuhmani
D. caniculata
W. baltica
D. algeriana
Pa. appenninica, P. buxtorfi
E. turriseiffelii
C. conica
N. convexa
A. albianus
P. praebuxtorfi
E. floralis
R. irregularis
Planktic foraminifera zones
Calcareous nannofossil zones
Age
Turonian
upper Cenomanian
Albian
Aptian
R. cushmani
Pa. appen.
Ps. tic.
NC 10
9
NC 7-8
NC 6
A

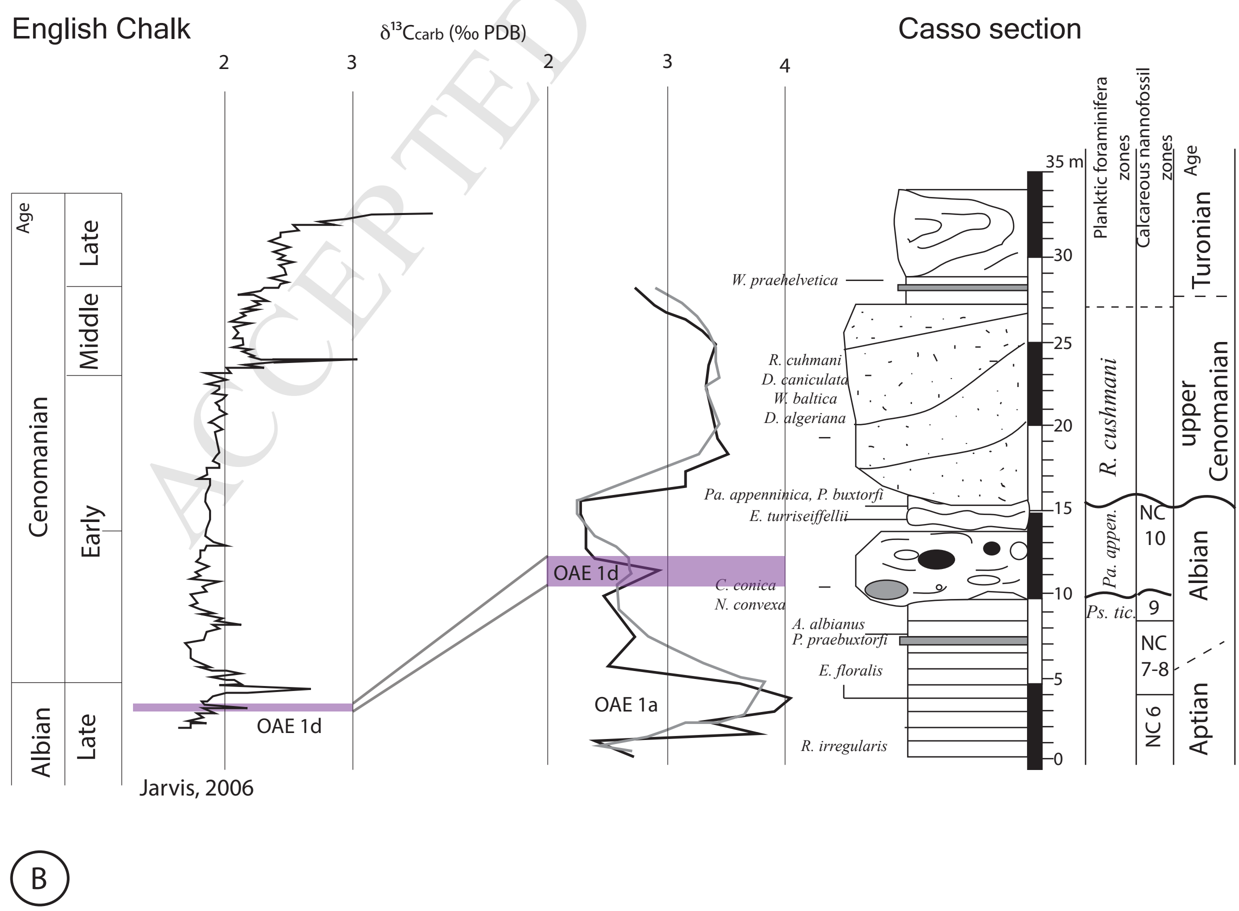

English Chalk
δ13Ccarb (‰ PDB)
2
3
4
Age
Cenomanian
Albian
Late
Middle
Early
Late
OAE 1d
Jarvis, 2006
Casso section
35 m
30
25
20
15
10
5
0
W. praehelvetica
R. cuhmani
D. caniculata
W. baltica
D. algeriana
Pa. appenninica, P. buxtorfi
E. turriseiffelii
C. conica
N. convexa
A. albianus
P. praebuxtorfi
E. floralis
R. irregularis
OAE 1d
OAE 1a
Planktic foraminifera zones
Calcareous nannofossil zones
Age
Turonian
upper Cenomanian
Albian
Aptian
R. cushmani
Pa. appen.
Ps. tic.
NC 10
9
NC 7-8
NC 6
B

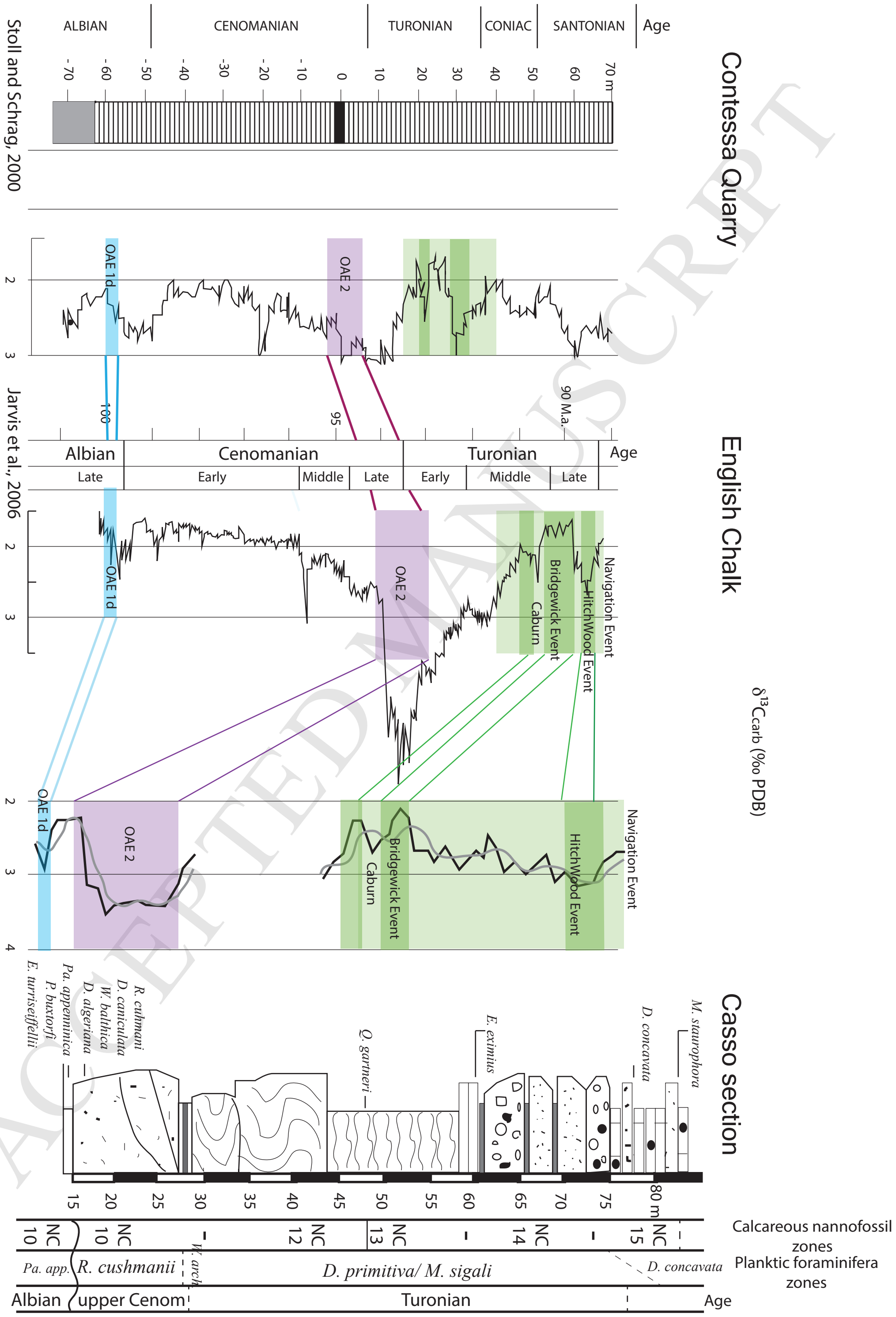
Contessa Quarry
Stoll and Schrag, 2000
ALBIAN
CENOMANIAN
TURONIAN
CONIAC
SANTONIAN
Age
70 m
OAE 1d
OAE 2
English Chalk
Jarvis et al., 2006
90 M.a.
95
100
Albian
Cenomanian
Turonian
Late
Early
Middle
Navigation Event
HitchWood Event
Bridgewick Event
Caburn
$\delta^{13}C_{carb}$ (‰ PDB)
Casso section
R. cushmani
D. caniculata
W. bathica
D. algeriana
Pa. appenninica
P. buxtorfi
E. turriseiffellii
Q. gartneri
E. eximius
D. concavata
M. staurophora
80 m
Calcareous nannofossil zones
Planktic foraminifera zones
NC 10
NC 12
NC 13
NC 14
NC 15
Pa. app.
R. cushmanii
W. arch.
D. primitiva/ M. sigali
D. concavata
Albian
upper Cenom
Turonian